MITSUBISHI ELECTRIC RESEARCH LABORATORIES
http://www.merl.com

Revisiting the State of Charge Estimation for Lithium-Ion Batteries A Methodical Investigation of the EKF Approach

Wang, Y.; Fang, H.; Zhou, L.; Wada, T.

TR2016-137 October 2016

Abstract

This article is devoted to nonlinear state and parameter estimation problems where the system is represented in the state-space framework. This article comprises of two parts where the first part provides a tutorial on prevailing nonlinear stochastic estimation techniques, and the second part presents a self-contained description of estimation problems and solutions in rechargeable Lithium-ion batteries.

IEEE Control Systems Magazine

This work may not be copied or reproduced in whole or in part for any commercial purpose. Permission to copy in whole or in part without payment of fee is granted for nonprofit educational and research purposes provided that all such whole or partial copies include the following: a notice that such copying is by permission of Mitsubishi Electric Research Laboratories, Inc.; an acknowledgment of the authors and individual contributions to the work; and all applicable portions of the copyright notice. Copying, reproduction, or republishing for any other purpose shall require a license with payment of fee to Mitsubishi Electric Research Laboratories, Inc. All rights reserved.

Copyright © Mitsubishi Electric Research Laboratories, Inc., 2016
201 Broadway, Cambridge, Massachusetts 02139

Revisiting the State of Charge Estimation for Lithium-Ion Batteries

A Methodical Investigation of the EKF Approach

Yebin Wang, Huazhen Fang, Lei Zhou, and Toshihiro Wada

With high energy/power density, flexible and lightweight design, low self-discharge rates and long lifespan, Lithium-ion (Li^+) batteries have experienced a surging growth since being commercialized in early 1990s [1]. They have established a dominance today in the consumer electronics sector, with several billions of them being used to power cellphones, cameras, laptops and tablets. Due to continually declining manufacturing costs, they are also rapidly penetrating into sectors such as grid, renewable energy, automotive and aerospace, where large-scale energy storage is needed. Looking into the future, the role of Li^+ batteries will be further strengthened as a key energy-storage technology to support the progression of the world into the green-energy era. However, their vulnerability to overcharging, overdischarging and overheating can easily expose them to performance degradation, shortened cycle life, and even fire and explosion, thus raising many concerns about their application. This challenge has been driving a massive solution-seeking effort in various research fields. Associated with this trend is the advancement of battery management systems (BMSs).

A BMS monitors the states and parameters of batteries, regulates the charging/discharging processes, and performs balancing across battery cells in order to meet the power demands, enhance safety and performance, and extend the lifespan. Among the tasks, the state of charge (SoC) monitoring is particularly important. The SoC, representing the amount of remaining charge in a battery, cannot be directly measured but is crucial for eliminating the threats of overcharging and overdischarging. This fact has thus stimulated an ongoing quest for high-caliber estimation strategies. Nevertheless, the evolution of SoC through time is based on complex nonlinear dynamic processes corresponding to thermodynamics, electrode kinetics, and transport phenomena. As a result, SoC monitoring involves, at its core, solving nonlinear estimation problems and has been very actively researched in the last decade. An overview of the state of the art is presented in Sidebar 1 "A survey of state of charge estimation".

This article presents a self-contained study of the SoC estimation problem for Li^+ batteries and solutions based on the extended Kalman filter (EKF). The EKF is arguably the most celebrated nonlinear estimation approach, and in recent years, its popularity has extended to battery management research. Now it is widely acknowledged in the literature as among the most competent techniques for SoC estimation. Its application to this subject, however, is not conclusive yet. The present literature has focused more on the use of the EKF technique, with less emphasis on the observability and sensitivity analysis critical for a successful estimation. The consequence is that some potential problems or pitfalls can escape notice—for instance, some unknown and weakly observable parameters can potentially compromise the accuracy of the full state estimation without any awareness. To remedy this issue, this study systematically demonstrates how the nonlinear estimation theory can be effectively exploited to understand the risks and challenges underlying accurate SoC estimation and build insights into improving

the prevailing estimation methods. With a brief description of Li^+ battery fundamentals and modeling, a thorough observability and sensitivity analysis is performed to illustrate the potential pitfalls that may fundamentally undermine the effectiveness of SoC estimation. Specifically, it is found that adaptive SoC estimation can be susceptible to a fundamental limitation plaguing adaptive systems: weak observability due to over-parametrized models and poorly informative data. Rooted in the observability/sensitivity analysis, the notion of parameter subset selection is leveraged to single out the most identifiable parameters, thus having the weak observability issue circumvented. Correspondingly, a new enhanced adaptive SoC estimator, consisting of two reduced-order EKFs running in the cascade mode, is developed. Additionally, a two-stage EKF is presented to reduce the computational cost of the joint EKF-based SoC estimator. All estimators are validated by synthetic and/or experimental data. The validation results agree with the outcomes drawn from the analysis. This article is concluded by a summary and an outlook to future work.

Li^+ Batteries and the Modeling

Preliminaries of Li^+ Batteries

A schematic description of a Li^+ battery cell is shown in Fig. 1. A cell is composed of four main elements: the positive electrode, negative electrode, electrolyte and separator. The positive electrode is typically made from Li^+ compounds, for instance, $Li_xMn_2O_4$ and Li_xCoO_2. Small solid particles of the compounds are compressed together, yielding a porous structure. The negative electrode is porous as well but usually made of graphite particles. The interstitial pores

at both electrodes create intercalation space, where the Li^+ ions can be moved in and out and stored. The electrolyte contains free ions and is electrically conductive, in which the Li^+ ions can be transported easily. The separator, separating the electrodes apart, allows the migration of Li^+ ions from one side to the other, but prevents electrons from passing through. The electrons are thus forced to flow through the external circuit. During the charging process, Li^+ ions are extracted from particles at the positive electrode into the electrolyte and then transported to the negative electrode absorb Li^+ ions through the electrolyte. This process not only generates an influx of Li^+ ions within the battery, but also builds up a potential difference between the positive and negative electrodes. Discharging is based on the reversed process. The following equations exemplify the chemical reactions in the positive and negative electrodes:

$$\mathrm{Li}_x\mathrm{Mn}_2\mathrm{O}_4 \underset{\text{discharge}}{\overset{\text{charge}}{\rightleftharpoons}} \mathrm{Li}_{x-y}\mathrm{Mn}_2\mathrm{O}_4 + y\mathrm{Li}^+ + y\mathrm{e}^-,$$

$$x\mathrm{Li}^+ + x\mathrm{e}^- + \mathrm{C} \underset{\text{discharge}}{\overset{\text{charge}}{\rightleftharpoons}} \mathrm{Li}_x\mathrm{C}.$$

The above working mechanism has been naturally abstracted into a diversity of spatially two-dimensional (2D) electrochemical models, among which are the Doyle-Fuller-Newman (DFN) model and its variants [2]–[4]. The 2D electrochemical models provide a high fidelity characterization of underlying physical and chemical processes, which makes them suitable for battery design and analysis. Though providing excellent physical insights, the 2D electrochemical models are hardly adopted in real-time BMSs, largely due to the prohibitive computation and onerous calibration. This weakness has been significantly relaxed by the single particle model (SPM) and its extensions [5]–[8], which simplify the 2D electrochemical models to one spatial dimension. Specifically, the SPM is derived by neglecting the electrolyte dynamics and treating each electrode as a spherical particle which stores Li^+. The SPM is valid for low to medium

charge/discharge currents (up to 1 C-rate) [6], [7]. While the SPM enjoys remarkable reduction of computation and calibration efforts in contrast to the 2D electrochemical models, it remains computationally expensive for real-time battery management with a representation based on partial differential equations (PDEs).

Instead of focusing on the electrochemical principles, many other threads of battery models have been developed according to different needs. In particular, equivalent circuit models (ECMs) have gained wide popularity among control engineers, representing a model class most useful for BMS design and implementation [9]–[13]. ECMs are intended to replicate the battery's input-output characteristics or in other words, emulate how charge/discharge currents influence the terminal voltage. A straightforward tool to understand and deduce the ECMs is the Thévenin's Theorem in circuit theory. The resultant Thévenin-based model consists of a series resistor, an RC circuit, and a voltage source, and is found capable of accurately predicting the transient response of the battery. Readers are referred to [11]–[13] for comparative studies of various ECMs. Overall, ECMs are among the most advantageous for embedded BMS development and will serve as a basis for SoC estimation in this article.

This article defines the terminology from a user perspective: treating the battery as an electric power source. The battery is considered to be fully charged and discharged when, with small charge and discharge currents, its terminal voltage reaches certain upper and lower thresholds. For the $LiFePO_4$-type cell used in the authors' experiment (to be presented later), it reaches full charge or discharge if its terminal voltage crosses 4.2Volt and 2.4Volt. A battery's nominal capacity is the amount of charge that it can take when brand new. The maximum capacity is the amount of charge that can be extracted from a fully charged battery. The state of

charge (SoC) represents energy available in a battery. Typically quantified by the ratio between the remaining amount of charge and the maximum capacity, the SoC takes values in $[0, 1]$. The state of health (SoH) indicates the capacity fading as a battery's maximum capacity will decrease gradually throughout the charge and discharge cycles. In general understanding, the capacity fading is attributed to unwanted side reactions including electrolyte decomposition, active material dissolution, and passive film formation. Accordingly, the SoH can be associated with or represented by different quantities, such as the ratio of the maximum capacity to the nominal capacity or the battery impedance indicating the film formation. The open circuit voltage (OCV), is the terminal voltage of the battery when it is cut off from the load. The OCV is uniquely determined by the SoC because the OCV corresponds to the difference between electrostatic potentials of the negative and positive electrodes, and the electrostatic potential of an electrode is determined by the quantities of Li^+ ions stored in the electrode [7]. The red dash dot line in Fig. 2 shows the OCV curve of the battery cell used in the experiments.

Batteries have many interesting but complicated phenomena: capacity fading, self-discharge, relaxation, hysteresis, the SoC-OCV curve, current-voltage characteristics, etc. Self-discharge represents the fact that the remaining charge stored in a battery will deplete over time. Depending on the cell chemistry, self-discharge could take up to years [14]. Relaxation is the change of the terminal voltage after the battery is disconnected from the load. The relaxation effect results from the Li^+ diffusion that continues even after the cell is cut off from the external circuit and can take up to hours. The hysteresis is generally referred to the phenomenon that: during a discharge, the battery terminal voltage always relaxes to a value less than the true OCV, and during a charge, the battery terminal voltage always relaxes to a value greater than the true OCV [9]. Fig. 2 shows the hysteresis effect of the battery cell used in the experiment. Note that

batteries with different chemistry could have these characteristics at different levels.

An Equivalent Circuit Model

This article considers a battery model shown in Fig. 3. It combines the Thévenin-based ECMs [11] with the hysteresis voltage dynamics [9]. The former offers a grasp of dynamic current-voltage characteristics, and the latter compensates the static current-voltage property. The model, striking an adequate balance between fidelity and simplicity, is given by

$$\begin{aligned} \dot{x}^1 &= -\alpha I, \\ \dot{x}^2 &= -\frac{1}{R_d C_d} x^2 + \frac{I}{C_d}, \\ \dot{x}^3 &= -\gamma |I| \left[\operatorname{sign}(I) V_{hs}(x^1) + x^3 \right], \\ y &= h(x^1) - x^2 + x^3 - R_s I, \end{aligned} \tag{1}$$

where x^1 is the SoC, x^2 the voltage cross the RC circuit, x^3 the hysteresis voltage, I the current in discharging ($I > 0$) or charging ($I < 0$), y the terminal voltage, $V_{hs}(x^1)$ the equilibrium of the hysteresis voltage dynamics, and $h(x^1)$ represents the SoC-OCV relationship. The model (1) includes parameters α, R_d, C_d, R_s and γ, where $\alpha = 1/(3600 C_0)$ with C_0 the maximum capacity, γ is the inverse of the hysteresis voltage dynamics time constant, and R_s, R_d and C_d are as defined in Fig. 3. The function $\operatorname{sign}(I) = 1$ for $I \geq 0$ and -1 otherwise. Here, the self-discharge phenomenon is not considered, because it is very slow for Li^+ batteries and has a negligible influence on state. The capacity fading can be reflected by the change in α. However, it is also a slow process, at rates several orders smaller than the battery state evolution. This implies that α can be treated as a constant during the SoC estimation. The thermal effects are not explicitly included in the battery model (1), but their effects can arguably be compensated

by adjusting model parameters.

In sequel, the following notation will be adopted for a vector ζ. Its i-th element is denoted by ζ^i. At the k-th time step, the i-th element is represented by ζ_k^i, and the j-th power of ζ_k^i is denoted as $(\zeta_k^i)^j$.

Offline Model Calibration

The battery model (1) must be calibrated prior to SoC estimation due to the presence of $V_{hs}(x^1)$, $h(x^1)$ and unknown parameters. Calibration of α can be achieved by depleting and then fully charging the battery with small currents. Impedance parameters R_d, C_d, R_s can be calibrated by: 1) injecting zero-mean current signal into the battery and collecting the input and output data; 2) linearizing the model (1) around a certain equilibrium $x_e = [x_*^1, 0, 0]^\top$ to obtain a linear time-invariant (LTI) model with linear parametrizations; 3) following standard procedures to identify parameters [11], [15], [16]. While offline adaptation is straightforward to understand and execute, online adaptation of all parameters is usually preferred. This is true for α because its offline calibration can be rather time-consuming and even unrealistic for some practical applications. The same observation extends to the other parameters as they vary with the current, SoC, and temperature indeed.

Specifically, when small constant charge and discharge currents are applied to the battery model (1), the voltage across the RC circuit and the hysteresis dynamics will both reach equilibria. According to the state equation of the battery model (1), these equilibria can be described as odd functions of the current. Therefore, the true SoC-OCV data can be derived as the average of the charge and discharge SoC-OCV curves.

Next is to parametrize the functions $h(x^1)$ and $V_{hs}(x^1)$, which has been studied by many researchers and often relies on a battery's energy storage dynamics. As an example, work [11] proposes $h(x^1) = a_0 \exp(a_1 x^1) + a_2 + a_3 x^1 + a_4 (x^1)^2 + a_5 (x^1)^3$, where a_j for $0 \leq j \leq 5$ are unknown parameters; in work [17], $h(x^1)$ is parametrized by $a_0 \log(x^1 + a_1) + a_2$; work [9] takes the Nernst parametrization $h(x^1) = a_0 + a_1 \log(x_1) + a_2 \log(1 - x^1)$. Parametrization of $h(x^1)$ ought to be determined in a way such that it can predict the true SoC-OCV curve and give rise to a simple expression of the hysteresis voltage $V_{hs}(x^1)$. Ideally, the equilibrium of $V_{hs}(x^1)$ can be represented as a constant so as to allow for a decoupling from x^1 [9]. However, this is not the case for the battery used in the experiment according to the SoC-$V_{hs}(x^1)$ plot shown in Fig. 2. Figs. 4-5 illustrate how to choose the parametrization of $h(x^1)$. As shown in Fig. 4, with a fixed x^1 and the parametrization #1, $V_{hs}(x^1)$ is not an odd function of I. With the parametrization #1, it necessitates two individual functions of $V_{hs}(x^1)$ for the charge and discharge processes. On the contrary, with the parametrization #2, $V_{hs}(x^1)$ is virtually an odd function of I, and thus can be represented by one simple function, $V_{hs}(x^1) = s(1 - x^1)$, for both charge and discharge processes. Fig. 5 verifies that the $\hat{V}_{hs}(x^1)$, if parameterized by $s(1 - x^1)$ with $s = 0.0755$, fits the measured data to a high precision.

State of Charge Estimation in Batteries

A BMS achieves a safe and efficient utilization of batteries only when it maintains accurate estimation of the battery state and parameters including the SoC and SoH. Given the nonlinear battery model and measurements, the SoC and SoH estimation problems can be formulated as nonlinear state and parameter estimation, respectively. The rest of this article will

focus its scope the SoC estimation. This is because state and parameter estimation will be mingled and can be addressed in the same framework or through similar estimation techniques [15], [18]. As such, a focus on the SoC estimation will still put SoH estimation in perspective, without compromising the value and contribution of this article.

In this section, both non-adaptive and adaptive SoC estimation problems will be examined on the basis of a thorough observability and sensitivity analysis. Baseline and new EKF-based SoC estimators will be provided and validated by using both simulation and experimental data. Synthetic data for simulation are generated from the battery model (1) with parameters: $C_0 =$ 4.9302Ah, $R_d = 3 \times 10^{-3}$ohm, $C_d = 9 \times 10^3$F, $\gamma = 2.47 \times 10^{-3}$, $s = 0.0755$, $R_s = 5 \times 10^{-3}$ohm. Experimental data are collected from a 18650-type Li^+ battery cell run on a battery tester located in the Advanced Technology R&D Center, Mitsubishi Electric Corporation. The battery has a nominal capacity of 4.9302Ah. The sampling period is $T_s = 1$sec. During the experiment, the ambient temperature in the chamber was maintained at 25.8°C. Throughout this section, the default units for voltages and currents are Volt and A, respectively. The battery capacity is given in the unit ampere-hour Ah. While the performance of estimators can be assessed on multiple criteria including the root-mean-square error and the ∞-norm of the estimation error signal, it is known that all norms are equivalent in some sense, so the ∞-norm of the SoC estimation error is adopted as the single criterion here for the sake of simplicity.

Non-Adaptive State of Charge Estimation

Dynamic model-based non-adaptive SoC estimation is to reconstruct the SoC without parameter adaptation, based on the battery model (1) and the current and voltage measurements.

Observability analysis of the battery model (1) establishes that (i) the battery model (1) is not uniformly observable; (ii) with a constant control, the battery model (1) is observable almost over the entire range of the SoC. Subsequently, the EKF is applied to solve the non-adaptive SoC estimation problem. Validation using the synthetic and experimental data reveals that the EKF estimator performs well with exact model knowledge, but fails to provide accurate estimation in the presence of the model-plant mismatch.

Uniform Observability Analysis

Uniform observability is of great importance as a prerequisite for applying diverse nonlinear observer design tools [19], [20]. It also often comes as a critical condition to establish the convergence of estimation error dynamics. Readers are referred to Sidebar 4 for details on uniform observability for nonlinear single input and single output affine control systems. The state equation of the battery model (1) admits the form

$$\dot{x} = f(x) + g(x, \text{sign}(I))I,$$

where $x = [x^1, x^2, x^3]^\top$, a smooth vector field $f(x) = [0, -x^2/\tau_d, 0]^\top$ with $\tau_d = R_d C_d$, and a non-smooth vector field $g(x, \text{sign}(I)) = \left[-\alpha, 1/C_d, -\gamma[(1-x^1)s + \text{sign}(I)x^3]\right]^\top$. With $I = 0$, the battery model (1) is reduced to the following uncontrolled form

$$\begin{aligned} \dot{x} &= f(x), \\ y &= h(x^1) - x^2 + x^3. \end{aligned} \tag{2}$$

A necessity for the model (1) to be uniformly observable is that the uncontrolled model (2) is observable. For the latter, the observable coordinates $\phi(x) = [y, L_f y, L_f^2 y]^\top$ are expressed by

$$y = h(x^1) - x^2 + x^3,$$

$$L_f y = x^2/\tau_d,$$

$$L_f^2 y = -x^2/\tau_d^2,$$

where $L_f \kappa(x)$ is the *Lie* derivative of the smooth function $\kappa(x)$ along the vector field f. The Jacobian of the observable coordinates, also referred to as the observability matrix $Q_o(x)$, is singular. The uncontrolled model (2) is not state observable, and thus the battery model (1) is not uniformly observable.

An interpretation of the unobservable space can be acquired by considering the following LTI system

$$\begin{aligned} \dot{\bar{x}} &= \begin{bmatrix} 0 & 0 & 0 \\ 0 & -1/\tau_d & 0 \\ 0 & 0 & 0 \end{bmatrix} \bar{x}, \\ \bar{y} &= [c_1, -1, 1]\bar{x}, \end{aligned} \tag{3}$$

where $\bar{x} = x - x_e$, $x_e = [x_*^1, 0, 0]^\top$ with $x_*^1 \in [0,1]$, and $c_1 = \frac{\partial h(x^1)}{\partial x^1}|_{x_*^1}$. The system (3) is derived from the linearization of the uncontrolled model (2) around x_e. For an n-dimensional LTI system

$$\begin{aligned} \dot{\zeta} &= A_\zeta \zeta + B_\zeta u, \\ y &= C_\zeta \zeta, \end{aligned} \tag{4}$$

where $\zeta \in \mathbb{R}^n$, the state observability can be examined by verifying the rank condition: $\text{rank}([\lambda \mathbf{I}_n - A_\zeta^\top, C_\zeta^\top]^\top) = n$ for all eigenvalues λ of A_ζ. Note that $\mathbf{I}_n$ is the $n \times n$ identity matrix. Regarding system (3), the rank condition is violated for the eigenvalue $\lambda = 0$. Hence, the unobservable space constitutes an eigenvector corresponding to the eigenvalue $\lambda = 0$.

The observable subspace of the uncontrolled model (2) can also be established. According to [21, Def. 3.29], the observable space is the linear space (over $\mathbb{R}$) of functions $h(x^1) - x^2 + x^3$

and x^2. Similarly, based on [21, Prop. 3.34], the unobservable submanifold is derived as $S_0 = \{x|h(x^1)-x^2+x^3=0, x^2=0\}$. Physical interpretation of the unobservable submanifold is evident: with $I=0$, both the hysteresis voltage x^3 and the OCV stay constant, but only their sum can be inferred from the output. Hence, x^1 and x^3 are indistinguishable.

Observability Analysis: Constant Control Case

In demonstrating the basis procedure for observability analysis, the above shows that zero control input will render the battery model (1) unobservable. However, this does not imply the infeasibility of SoC estimation. Since the SoC estimation is meaningful during the battery operation, it is more relevant to investigate whether the battery model (1) is observable when practical control inputs exist. Similar problems have been studied for general non-affine control systems [22]. Observability analysis can be performed when the battery model (1) is subject to a specific form of control inputs.

For illustration purposes, this section demonstrates the observability analysis when the battery model (1) is subject to constant control inputs. Without loss of generality, assume $I = I_0 > 0$ with I_0 constant. The battery model (1) is rewritten as $\dot{x} = f(x), y = h(x^1)-x^2+x^3-R_sI_0$ with $f(x) = \left[-\alpha I_0, -x^2/\tau_d + I_0/C_d, -\gamma I_0[(1-x^1)s+x^3]\right]^\top$. The observable coordinates are

$$
\begin{aligned}
y &= h(x^1)-x^2+x^3-R_sI_0,\\
L_f y &= -\alpha I_0 \frac{\partial h(x^1)}{\partial x^1} + \frac{x^2}{\tau_d} - \frac{I_0}{C_d} - \gamma[s(1-x^1)+x^3],\\
L_f^2 y &= \alpha I_0 \left[\alpha I_0 \frac{\partial^2 h(x^1)}{\partial (x^1)^2} - \gamma s\right] - \frac{x^2}{\tau_d^2} + \frac{I_0}{\tau_d C_d} + \gamma^2\left[s(1-x^1)+x^3\right],
\end{aligned}
$$

and the observability matrix is given by

$$Q_o(x, I_0) = \begin{bmatrix} \frac{\partial h(x^1)}{\partial x^1} & -1 & 1 \\ \gamma s - \frac{\partial^2 h(x^1)}{\partial (x^1)^2} \alpha I_0 & \frac{1}{\tau_d} & -\gamma \\ \alpha^2 I_0^2 \frac{\partial^3 h(x^1)}{\partial (x^1)^3} - \gamma^2 s & -\frac{1}{\tau_d^2} & \gamma^2 \end{bmatrix}.$$

The determinant of the observability matrix is $\det(Q_o) = 1/\tau_d^2 \rho(x^1)(\gamma\tau_d - 1)$, where

$$\rho(x^1) = \frac{\partial^3 h(x^1)}{\partial (x^1)^3} \alpha^2 \tau_d I_0^2 - \alpha I_0 \frac{\partial^2 h(x^1)}{\partial (x^1)^2} (\gamma\tau_d + 1) + \frac{\partial h(x^1)}{\partial x^1} \gamma + \gamma s.$$

The observability matrix is singular if and only if one of the following facts holds:

(i) $\gamma\tau_d = 1$. This fact holds only if the RC circuit and the hysteresis voltage dynamics have exactly the same time constant, which is unlikely in practice.

(ii) $\rho(x^1) = 0$. This fact imposes conditions on the function $h(x^1)$. With $\frac{\partial^3 h(x^1)}{\partial (x^1)^3} > 0, \frac{\partial^2 h(x^1)}{\partial (x^1)^2} < 0, \frac{\partial h(x^1)}{\partial (x^1)} > 0$ for almost all $x^1 \in [0, 1]$, as shown in Fig. 6, one immediately has $\rho(x^1) > 0$.

The battery model (1) with non-zero constant controls is therefore observable for almost all $x^1 \in [0, 1]$. The non-singular observability matrix is however not enough to guarantee accurate state estimation, because the state estimation performance can be compromised by the existence of weakly observable modes [23], [24]. A linear system is weakly observable if the observability matrix is ill-conditioned. Similar criteria have been used for nonlinear systems [25]. Unlike linear systems, the observability matrix of a nonlinear system often depends on control inputs. A common practice is to check the observability matrix for a given control input. As an example, the observability matrix of the battery model (1) is checked for a constant current input $I = 2$C-rates, with the condition number plotted in Fig. 7. The observability matrix has the condition number at the order of 10^4. Despite a possible issue for a high dimensional matrix, the condition

number of around 10^4 is not a problem for a 3×3 matrix [26]. The non-adaptive SoC estimation problem is therefore well-posed.

Observability analysis of the battery model (1) can be alternatively conducted in nonlinear switched system setting, since the model (1) can be reformulated as a switched system with $g(x,\text{sign}(I)) = \left[-\alpha, 1/C_d, -\gamma[(1-x^1)s+x^3]\right]^\top$ for $I \geq 0$ and $g(x,\text{sign}(I)) = \left[-\alpha, 1/C_d, -\gamma[(1-x^1)s-x^3]\right]^\top$ otherwise. Interested readers are referred to [27] for details.

Applicability of the Extended Kalman Filter

The aforementioned observability analysis manifests that the battery model (1) is not transformable to special structures as required by normal form-based observer designs [19], [22], [28]–[36]. In addiiton, deficiency of uniform observability defies a large portion of nonlinear observer designs. On the contrary, nonlinear stochastic estimation techniques do not impose such restrictions on the system structure. The incentive to explore the SoC estimation in the stochastic framework is further strengthened by the necessity to accommodate sensor and actuator noises. Thus in this regard, nonlinear stochastic estimators such as the EKF, the unscented Kalman filter (UKF) [37], [38], the Ensemble Kalman Filter (EnKF) [39]–[41], and the particle filter [42] are preferable thanks to the capability of dealing with noises and quantifying uncertainties and confidence intervals of the estimates. Compared with the particle filter and the moving horizon estimator [43], the EKF and its variants, the UKF and the EnKF, are attractive for the relatively easy design and implementation and moderate computational expenses for low-order systems. This technique also suffers from several shortcomings such as performance degradation due to linearization-induced errors or non-Gaussian noises, lack of stability results, and hefty

computational costs for high-dimensional systems. Yet the advantages outweigh the disadvantages when low-dimensional stochastic systems as in many real-world applications are concerned, so the EKF is still a highly appealing tool, if not the most popular, among industrial practitioners. As such, the EKF is a competent solution to non-adaptive SoC estimation problem. A look at the noises and lineariziation error in the case of SoC estimation below corroborates this point.

Noises in sensors and actuators of the BMS mainly come from quantization errors, constant offsets, and noises due to power electronics. The constant offsets in sensors and actuators can be readily dealt with by introducing constant bias parameters in the estimator [23], [44]. Noises in power electronics are typically at much higher frequencies than the sampling frequency and the bandwidth of the battery dynamics, and thus are negligible. Concerning the quantization error, a plethora of research work towards analyzing the stochastic properties, and mitigating the adverse effects on feedback control systems. For instance, work [45] establishes necessary and sufficient conditions to ensure that the quantization error is white and additive. Work [46] establishes that the uniform quantization often leads to additive quantization errors with white spectrum. In work [47], effects of different quantization schemes on Kalman filter-based state estimation for LTI systems are analyzed; and demonstrates that certain quantization schemes render the output error $y-\hat{y}$ asymptotic Gaussian process, and thus validate Kalman filter-based state estimation. Thus it will not cause a loss of generality to assume that the quantizers have been designed to produce white and additive quantization errors. Last but not least, the detrimental effects of the linearization-induced error on the EKF-based SoC estimation are insignificant because

(i) the battery model (1) does not possess strong nonlinearity. Specifically, the state equation

is linear in the state; as shown in Fig. 6, the nonlinearity in the output equation has a gradient bounded by $[0.75, 3]$;

(ii) the model mismatch due to linearizing the output equation can be effectively alleviated by setting the initial SoC of the EKF estimator close to the true value. This is possible because the output y is dominated by the OCV and thus can be used to generate a good initial guess of the SoC.

Extended Kalman Filter-based State of Charge Estimation

To facilitate the EKF-based non-adaptive SoC estimation, the battery model (1) is discretized to give the following discrete-time model

$$\begin{aligned} x_{k+1} &= A_k(\theta, u_k)x_k + B_k(\theta, u_k)u_k + w_k^x, \\ y_k &= h(x_k^1) - x_k^2 + x_k^3 - \theta^5 I^k + v_k, \end{aligned} \tag{5}$$

where $\theta = [\theta^1, \cdots, \theta^5]^\top$, k is the time index, $u_k = [I_k; 1]^\top$, $w_k^x = [w_k^1, \ldots, w_k^3]^\top$ are process noises, and v_k is the measurement noise. The noise covariances are $W_k^x = E[w_k^x (w_k^x)^\top] = \text{diag}\{W_k^1, \ldots, W_k^3\}$, and $V_k = E[(v_k)^2]$. Matrices in (5) are given by

$$A_k(\theta) = \begin{bmatrix} 1 & 0 & 0 \\ 0 & \theta^2 & 0 \\ (1-(\theta^4)^{|I_k|})\text{sign}(I_k)s & 0 & (\theta^4)^{|I_k|} \end{bmatrix},$$

$$B_k(\theta) = \begin{bmatrix} -\theta^1 & 0 \\ \theta^3 & 0 \\ 0 & ((\theta^4)^{|I_k|} - 1)\text{sign}(I_k)s \end{bmatrix},$$

where $\theta^1 = \alpha T_s, \theta^2 = \exp(-T_s/\tau_d), \theta^3 = R_d(1-\theta^2), \theta^4 = \exp(-\gamma T_s), \theta^5 = R_s$, $s = 0.0755$, and $T_s = 1$sec the sampling period. For ease of presentation, x_k^1 is treated as a constant during the

discretization of the hysteresis voltage dynamics.

The sampling period is determined by the battery dynamics, the sensor resolution and computation resources. Given that the time constant of battery dynamics is typically longer than ten seconds [9], [11]–[13], the sampling period can be a few seconds. On the other hand, the sampling period should be long enough such that the data acquisition hardware in the BMS can produce accurate readings. This is primarily constrained by the sensor resolution, the impact of which can be exemplified by the voltage sensor. Based on the specification of the battery terminal voltage, the voltage sensor range can be selected as $[0,5]$Volt. With a 12-bit A/D converter, the resolution of the voltage sensor is $5/2^{12} = 0.0012$Volt. As pointed out in [48], typical electric vehicles and hybrid electric vehicles are ideally discharged at 1 C-rate and 3 C-rates. Assume that the battery is charged at 3 C-rates. The SoC increases at a rate of $0.084\%/$sec. Considering the gradient plot in Fig. 6, the terminal voltage increases at the rate ranging $[0.00063, 0.00252]$Volt$/$sec. The changes of the terminal voltage within a sampling period $T_s = 1$sec can be barely detected by the voltage sensor. A sampling period shorter than 1sec will be unnecessary.

Given the discretized model (5), the EKF design for the full state estimation is a straightforward exercise of results in Sidebar 2 and thus omitted. The EKF-based non-adaptive SoC estimator is first validated by synthetic data, which are generated by exciting the discretized model (5) with two current profiles: pulses and urban dynamometer driving schedule (UDDS). The initial conditions (ICs) of the battery model and the EKF estimator are taken as $x_0 = [0.95, 0.1, 10^{-3}]^\top$ and $\hat{x}_0 = x_0/2$, respectively. Tuning parameters of the EKF are taken as: $Q^x = 10^{-4}\mathbf{I}_3, R = 10^{-4}, P_0 = 0.5\mathbf{I}_3$. The EKF estimator is fairly robust to changes of Q, R, and

the tuning is straightforward. Simulation results for both the pulse and the UDDS current profiles are shown in Figs. 8-9. When both the model (5) and the EKF use the same values of model parameters, the SoC estimates converge to the true states. With model parameters 20% off the true values, the EKF could not give convergent SoC estimates.

The EKF-based non-adaptive SoC estimator is further validated by experimental data, with results shown in Fig. 10. It reveals that the SoC estimation is unsatisfactory. This is because the values assigned to the parameters may differ from the truth. Since no parameter adaption is exploited here, the model mismatch remains throughout the entire estimation process. This implies the necessity of integrating a parameter adaption mechanism in order to improve the SoC estimation accuracy.

Adaptive State of Charge Estimation

As shown above, non-adaptive SoC estimation is near a failure in the experimental validation. This does not come as a surprise, because the simulation is premised on accurate parameters, and by contrast, an exact knowledge about battery parameters is absent in practice. Even worse, the battery's parameters can fluctuate with the input current, the SoC, and the battery temperature. Adaptive SoC estimation, hence, is of considerable importance in the real-world battery use, with its capability of updating the parameter values in real time to provide a better model. This section offers a series of EKF-based adaptive SoC estimators. For self-completeness and comparison purposes, a baseline joint EKF estimator is first presented to expose its weakness: the relatively high computational cost and tremendous tuning efforts. The high computation cost is alleviated by leveraging a two-stage EKF described in Sidebar 3. The tuning difficulty is

addressed by sensitivity analysis which singles out a set of most identifiable parameters to exclude weakly observable modes. Based on the sensitivity analysis, an enhanced adaptive SoC estimator is developed. Finally, simulation and experiments demonstrate the effectiveness of both the enhanced adaptive SoC estimator and the two-stage EKF design.

Joint Extended Kalman Filter Approach

Joint EKF frequently appears as a viable solution to many applications involving state and parameter estimation. A comprehensive description of its application to adaptive SoC estimation is presented in [49]. The joint EKF-based adaptive SoC estimator is based on the following augmented battery model

$$x_{k+1}^a = \begin{bmatrix} A_k(\theta_k, u_k)x_k + B_k(\theta_k, u_k)u_k \\ \theta_k \end{bmatrix} + \begin{bmatrix} w_k^x \\ w_k^\theta \end{bmatrix}, \tag{6}$$
$$y_k = h(x_k^1) - x_k^2 + x_k^3 - \theta_k^5 I_k + v_k,$$

where $x_k^a = [x_k^\top, \theta_k^\top]^\top \in \mathbb{R}^8$ is the augmented state, and $w_k^\theta = [w_k^4, \ldots, w_k^8]^\top$ with the covariance matrix $W_k^\theta = E[w_k^\theta (w_k^\theta)^\top] = \text{diag}\{W_k^4, \ldots, W_k^8\}$. The augmented battery model (6) is derived from treating battery parameters constant. Such a treatment is arguably valid when battery parameters vary much slower than the sampling period. Fluctuations of the temperature and SoC are typically slow, and thus their influences on battery parameters can be characterized by the term w_k^θ. The covariance of w_k^θ should reflect how fast parameters change over time. The charge rate might change faster than the sampling rate, and the resultant parameter variations cannot be captured by the model (6). This limitation however can be addressed by considering rate-dependent parameter models as in [11]. It is not theoretically justifiable to assume a diagonal

W_k^θ, because the components of w_k^θ are induced by the temperature variation and thus correlated. Non-diagonal W_k^θ might be addressed by adaptive EKFs that estimate the noise covariances along with the state, though the adaptive EKFs may suffer from weak observability in this case because of more unknown variables to estimate [50].

Given the augmented model (6), the joint EKF-based adaptive SoC estimator can be acquired according to Sidebar 2 and thus omitted here. While simulating the joint EKF-based adaptive SoC estimator with the synthetic data, its ICs and tuning parameters are given by

$$\begin{aligned}
&\hat{x}_0^a = [0.75x_0^\top, 0.8\theta_0^\top]^\top,\\
&Q = \text{diag}\{10^{-6}, 10^{-8}, 10^{-8}, 5\times 10^{-11}, 10^{-8}, 10^{-10}, 10^{-4}, 10^{-8}\},\\
&R = 10^{-4},\\
&P_0 = \text{diag}\{0.0625, 0.01, 10^{-6}, 10^{-10}, 0.0625, 10^{-7}, 0.0625, 10^{-3}\},
\end{aligned}$$

where $x_0 = [0.95, 0.1, 10^{-3}]^\top$ is the true state, and $\theta_0 = [6.94\times 10^{-5}, 0.989, 3.31\times 10^{-4}, 0.998, 0.08]^\top$ the true parameter values, computed according to true values of R_s, R_d, C_d, R_s, C_0. Simulation results are given in Fig. 11 for the pulse current, and Fig. 12 for the UDDS current. Simulation results for both current profiles lead to the following observations:

(i) Unlike the non-adaptive case, the joint EKF-based adaptive SoC estimator can provide accurate SoC estimation.

(ii) Significant efforts are required to tune the Q, P_0 to ensure the convergence of the state and parameter estimation. With slight changes of Q, P_0, the joint EKF might fail to converge. Parameters θ^2, θ^4 are much more difficult to estimate than other parameters. This is consistent with the sensitivity analysis to be offered below.

(iii) The adaptive SoC estimator takes longer to converge than the non-adaptive case. This is as expected due to the additional parameter identification process.

The joint EKF is also verified by the experimental data, as shown in Fig. 17. Both simulation and experimental studies confirm that the adaptive SoC estimation outperforms the non-adaptive case in terms of the estimation accuracy, though it should be noted that tuning of the joint EKF for adaptive SoC estimation is more time-consuming.

Fig. 7 plots the condition number of the observability matrix when the eighth order augmented model (6) is excited by a constant current. The observability matrix is nonsingular but ill-conditioned, which implies that the eighth order augmented model (6) is only weakly observable. The tuning difficulty of the joint EKF can be explained by the known result: the full state estimation performance can be dramatically compromised by the existence of weakly observable modes [23], [51]. Even for a strongly observable nonlinear system, the EKF tuning remains a challenging problem. Meanwhile, adaptive EKFs, aimed to alleviate the tuning efforts by online identification of noise covariance matrices, have been intensively investigated [50]–[52]. Such methods however can incur a significantly increased computation load, and thus their adoption to the BMS remains uncertain.

Performance of the EKF heavily depends on matrices Q, R and P_0. For linear systems, ideally, Q, R, P_0 are the covariances of the process noise, measurement noise, and initial state error. For nonlinear systems, the tuning of Q, R, P_0 is not straightforward and typically resorts to the trial-and-error approach, though existing work does establish some useful insights [53], [54]. A common tuning guideline is that Q, R should take into account linearization errors as well as noises [53]. Next shown is the tuning practice followed in the simulation. Denote a constant

matrix $Q = \text{diag}\{q^1, \cdots, q^8\}$. Guidelines to determine Q and R are illustrated by exemplifying the determination of q^1, q^8, R from the first state equation, the eighth state equation, and the output equation of the battery model (6). Assume that the noise covariance of the current source is $W_1^x = 10^{-4}$. Considering

$$\hat{x}_{k|k}^1 = \hat{x}_{k|k-1}^1 + K_k^1(y_k - \hat{y}_{k|k-1}) = -\hat{\alpha}_{k-1|k-1} I_k + \sqrt{q^1} + K^1(y_k - \hat{y}_{k|k-1}),$$

with K_k^1 the gain, and the true dynamics $x_k^1 = -\alpha_k(I_k + w_k^1)$, one will have

$$x_k^1 - \hat{x}_{k|k}^1 = -K_k^1(y_k - \hat{y}_{k|k-1}) - \underbrace{\left[(\alpha_k - \hat{\alpha}_{k-1|k-1})I_k + \alpha_k w_k^1\right]}_{d_k^1} - \sqrt{q^1}.$$

Let $q^1 = E[(d_k^1)^2]$ to compensate linearization errors and noises such that the estimation error dynamics are dominated by the term $-K_k^1(y_k - \hat{y}_{k|k-1})$. Considering that $(\alpha_k - \hat{\alpha}_{k-1|k-1}) \sim 10^{-5}$, $w_k^1 \sim 10^{-2}$, $I_k \sim 10$, the covariance of d_k^1 is in the order of 10^{-8}. Hence, q^1 should be taken a value around 10^{-8}. Conditions on q^2, q^3 can also be similarly derived. Differently, $q^4, \ldots, q^8$ are associated with parameter dynamics $\theta_{k+1}^i = \theta_k^i + w_k^i$, which is not subject to a linearization error. For $4 \leq i \leq 8$, q^i depends on the nominal value of the parameter θ^i, and how fast the parameter changes. Taking θ^5 as an example, its nominal value is around 10^{-3}. Assume that parameter θ^5 changes at a time constant of about one hundred seconds. Given the sampling period $T_s = 1$sec, one would like to tune q^8 such that the EKF can track the parameter within its time constant. That is to say, q^8 should be at the order of 10^{-10}. Similar idea is applicable to tune $q^4, \ldots, q^7$.

The matrix R accounts for uncertainties in $y_k - \hat{y}_{k|k-1}$: the linearization error and noises. Assume that the voltage sensor has a noise covariance 10^{-6}. With the Taylor series expansion of $h(x^1)$, $y_k - \hat{y}_{k|k-1}$ is approximated as

$$\left.\frac{\partial^2 h(x^1)}{\partial (x^1)^2}\right|_{\hat{x}_{k|k-1}^1} (x_k^1 - \hat{x}_{k|k-1}^1)^2 - (R_s)_k w_k^1 + v_k + \mathscr{O}((x_k^1 - \hat{x}_{k|k-1}^1)^2).$$

The first term is approximately at the same order as $(x_k^1 - \hat{x}_{k|k-1}^1)^2$ or 10^{-2}. Given $R_s \sim 10^{-3}$, $w_k^1 \sim 10^{-2}$, and $v_k \sim 10^{-3}$, the second and third terms are at the order of 10^{-5} and 10^{-3}, respectively. Overall, the order of the linearization error is 10^{-2}. This implies that R should be around 10^{-4}. Note that the above selection for Q and R is a worst-case design. In fact, as the EKF estimator converges, the linearization error decreases, which calls for a decline of Q and R accordingly. In the simulation, the matrices Q, R are set to be constant for simplicity. A similar tuning technique has been developed and applied to tune the EKF for chemical processes [55].

Two-stage Extended Kalman Filter Approach

A two-stage EKF based on the optimal two-stage Kalman filter (OTSKF) [56], [57] is designed and validated for the adaptive SoC estimation, aiming at balancing the computation complexity and estimation performance. The two-stage EKF is applied to the augmented battery model (6). Readers are referred to Sidebar 3 where a detailed design of the two-stage EKF for a nonlinear system is provided.

With the same ICs and tuning parameters, both the two-stage EKF and the joint EKF are validated by experimental data. The SoC estimation results are plotted in Fig. 14, where the two-stage EKF produces comparable performance as the joint EKF. The computational burden of the two-stage EKF and the joint EKF for the adaptive SoC estimation problem can be evaluated as in [56] and [57]. Given that the dimensions of the state, parameter, input, and output are $n_x = 3$, $n_\theta = 5$, $n_u = 1$, and $n_y = 1$, respectively, the two-stage EKF takes 558 fewer arithmetic operations per sample time than the joint EKF.

Sensitivity Analysis

When addressing an adaptive estimation problem, two important questions to ask are whether adaptive estimation is possible and how difficult it is. These questions can be answered by rigorous observability/identifiability analysis, which has been carried out in different ways. As a standard approach, the observability analysis can be performed on the augmented model (6). Provided that the observability matrix is non-singular and well-conditioned, the stable adaptive SoC estimation is possible [58, Lem. 2.2.4]. When the augmented model (6) is subject to a constant current input, the observability matrix Q_o is nonsingular. Analysis however demonstrates that Q_o is ill-conditioned, as shown in Fig. 7. In order to determine which parameter causes the ill-conditioning of Q_o, one augments the battery model (1) with different parameters and then examines the condition numbers of the augmented battery models. This procedure is tedious because it requires an exhaustive enumeration of all possible parameter sets, and the matrix Q_o is rather intricate. See [59] for an example of applying rigorous algebraic identifiability conditions to an HIV/AIDS model.

Another approach makes use of the sensitivity analysis to determine whether parameter variations can propagate to the output y. Sensitivity analysis is the study of how uncertainty in the model output can be apportioned to different sources of uncertainty in the model input [60]. Sensitivity analysis has been successfully applied to miscellaneous engineering problems: identify critical regions in the parameter space [60], determine the most identifiable subset of parameters to facilitate model reduction and parameter estimation, etc. Particularly, a multitude of recent works report how sensitivity analysis is exploited to choose the most significant parameters for diverse engineering systems, for instance, waste water treatment processes [61]–[63], the

activated sludge model [64], synchronous generators [65], [66], to name a few. Interested readers are referred to [60] for more information about sensitivity theory and applications. Compared with the observability analysis, sensitivity analysis is straightforward to troubleshoot an ill-posed estimation problem and thus is instructive in practice.

Sensitivity analysis can be employed to establish that the adaptive SoC estimation based on the augmented model (6) suffers from the fundamental limitation caused by the over-parametrized battery model and the limited data. It can further provide guidelines to bypass the limitation. For simplicity, local sensitivity analysis is performed, where small perturbations of parameters at specified nominal values are first assumed, and then the impact of the perturbations on the output is quantified [60], [63]. Regarding the augmented model (6), the sensitivity of y w.r.t. parameters can be derived

$$\begin{aligned}
&\frac{\partial y}{\partial \theta^1} = \frac{\partial h}{\partial x^1}\frac{\partial x^1}{\partial \theta^1} = -I\frac{\partial h}{\partial x^1},\\
&\frac{\partial y}{\partial \theta^2} = -\frac{\partial x^2}{\partial \theta^2} = -x^2,\\
&\frac{\partial y}{\partial \theta^3} = -\frac{\partial x^2}{\partial \theta^3} = -I,\\
&\frac{\partial y}{\partial \theta^4} = \frac{\partial x^3}{\partial \theta^4} = |I|\left(\theta^4\right)^{|I|-1}\left[x^3 + \mathrm{sign}(I)(1-x^1)s\right],\\
&\frac{\partial y}{\partial \theta^5} = -I.
\end{aligned} \tag{7}$$

Provided that $x^2 \ll 1, x^3 \ll 1, \theta^4 \approx 1$, and $s = 0.0755$, θ^2 and θ^4 barely affect y and are difficult to identify. This qualitative reasoning is affirmed by simulation results, which are shown in Fig. 13. Since the sensitivities of y w.r.t. θ^3 and θ^5 are equal to $-I$, Fig. 13 only plots $\partial y/\partial\theta^1$, $\partial y/\partial\theta^2$, and $\partial y/\partial\theta^4$, when the battery model (1) is subject to the pulse and the UDDS currents.

The aforementioned sensitivity analysis result can be nicely interpreted in adaptive framework [15]. Considering that the gain from the control input to x^1 is $1/(3600C_0) \ll 1$,

the state x^1 can be treated as a constant for a reasonably long time interval. Additionally, states x^2 and x^3 always stay in a small neighborhood of the origin. Within a reasonably long time interval, the battery state barely changes, and thus the battery model (6) can be treated as an LTI system. With this in mind, one can establish the strong connection between the sensitivity analysis result and the persistent excitation condition [15]. This is elucidated by studying a single input and single output LTI system (4), where A_ζ, B_ζ and C_ζ are unknown matrices. It is understood that system (4) can be transformed into another special form

$$\begin{aligned} \dot{x} &= Kx + B_y y + B_u u, \\ y &= Cx, \end{aligned} \tag{8}$$

where both K and C are known and in special structures [15]. Unknown parameters of system (8) only appear in B_y and B_u. With (8), a set of filters can be constructed to generate known signals $\psi(t)$ such that y takes a linear parametrization [15]

$$y(t) = \psi(t)\theta,$$

where $\theta = [B_y^\top, B_u^\top]^\top$ and $\psi(t) = [\psi^1(t), \ldots, \psi^{2n}]$. Applying local sensitivity analysis gives $\partial y(t)/\partial \theta^i = \psi^i(t)$, and concludes: a parameter θ^i is deemed critical only if the auxiliary signal $\psi^i(t)$ has a relatively large magnitude over $t \in [0, \infty)$. On the other hand, the persistent excitation condition requires there exist constants $0 < T < \infty$, $0 < \alpha < \beta < \infty$ such that $\alpha \mathbf{I}_{2n} \leq \int_t^{t+T} \psi^\top(\tau)\psi(\tau)\mathrm{d}t \leq \beta \mathbf{I}_{2n}$.

Sensitivity Analysis-based Extended Kalman Filter Approach

An enhanced adaptive SoC estimation scheme is provided to cut back the tuning work associated with the joint EKF. As a direct application of the sensitivity analysis, one selects a

subset of parameters to which the output is strongly sensitive, and augments the battery model (1) with the selected parameters instead of the entire set of parameters. Considering the demonstrated similarity between the sensitivity analysis result and the persistent excitation condition, such a scheme can find support from the adaptive theory: adaptive estimation of a higher order system requires richer excitation signals [15]. With the most identifiable parameters to estimate, conditions result from the sensitivity analysis are more likely satisfied. The scheme is also validated by performing the observability analysis on the fourth order battery model, which is obtained from augmenting the battery model (1) with an additional state α. With a constant current applied to the fourth order battery model, the condition number of the observability matrix is shown in Fig. 7. Compared with the eighth order augmented model, the observability matrix is significantly conditioned.

The aforementioned scheme is validated by conducting two studies based on experimental data. In the first study, a reduced order EKF-A is implemented to estimate the battery state x and two parameters: θ^1, θ^5. Results are shown in Fig.15. As anticipated, tuning of the EKF-A is a lot more straightforward. Several statements can be made from this study:

(i) The SoC estimation produced by the EKF-A is less accurate than the joint EKF case.

(ii) The EKF-A provides more consistent estimation of θ^1 and θ^5 than the joint EKF.

With an averaging window size of 1000 time steps, the EKF-A outputs parameter estimates: $\hat{\theta}_1 = 5.719 \times 10^{-5}$ and $\hat{\theta}_5 = 7.634 \times 10^{-4}$.

In the second study, a reduced order EKF-B is utilized to estimate the battery state and parameters $\theta^2, \theta^3, \theta^4$. Experimental results of the EKF-B are given in Fig. 16, from which the

following facts are observed:

(i) The SoC estimation from the EKF-B is not satisfactory. This is associated with the use of the incorrect maximum capacity value.

(ii) The SoC estimation accuracy of the EKF-B is dominated by the error between the α value used in the EKF-B and the true value.

(iii) The unknown parameters θ^2, θ^3 and θ^4 are still difficult to identify. This phenomenon is caused by their weak identifiability and agrees with the sensitivity analysis results.

With the aforementioned analysis and validation, the sensitivity analysis-based enhanced adaptive SoC estimation scheme is given as follows

(i) In the beginning, the EKF-A estimates the battery state and two parameters: θ^1 and θ^5.

(ii) After the EKF-A produces convergent parameter estimation, the EKF-B estimates the battery state and the rest parameters, using θ^1 and θ^5 from the EKF-A. The SoC produced by the EKF-B constitutes the final SoC estimate.

(iii) Both the EKF-A and EKF-B run in the cascade mode. Specifically, the EKF-B runs with the sampling period $T_s = 1$sec, and the EKF-A runs at a much slower time scale compared with the EKF-B. This arrangement is justified by the fact that both θ^1 and the parameter θ^5 change at a pace much smaller than T_s.

Experimental data are applied to validate the enhanced adaptive SoC estimation scheme, and results are compared with the joint EKF case. As shown in Fig. 17, the SoC estimation error of the enhanced adaptive scheme is about $\pm 1\%$ versus $\pm 2\%$ for the joint EKF case. Additionally, the enhanced adaptive scheme enjoys advantages such as a reduced level of efforts in tuning the

resultant EKFs, and a lower computational burden.

One of challenges that a real BMS faces is how to mitigate adverse effects that result from variations of the ambient temperature. This is important because the ambient temperature change the noise properties, and the battery model parameters. An ideal SoC estimator can either adapt to or reject the fluctuation of the ambient temperature. Improving the enhanced EKF by adapting Q and R to the ambient temperature can be part of the future work. Next two preliminary studies examine whether the enhanced EKF is robust against mismatches between true noise properties and tuning parameters Q and R. In the first study, with the matrices Q and R tuned simultaneously, the enhanced EKF is validated against experimental data. Fig. 18 compares the SoC estimation for four cases: the Q,R are 0.1, 1, 10, 100 times of the nominal values. Results in Fig. 18 demonstrate that with increased Q and R, the performance of the enhanced EKF barely changes; reduced Q and R do incur noticeable performance degradation. In the second study, only $q^4,\ldots,q^8$ are changed, and the enhanced EKF is verified by experimental data. For four cases, where $q^4,\ldots,q^8$ are set to 0.5, 1, 1.5 and 2 times of the nominal values, the enhanced EKF produces almost the same SoC estimation, as shown in Fig. 19. This study offers some confidence about the robustness of the enhanced EKF estimator with respect to the noise covariance mismatch, which can be caused by the fluctuation of the ambient temperature.

Conclusion and Future Work

This article offered an in-depth case study of nonlinear SoC estimation for Li^+ battery management. SoC monitoring is at the heart of an advanced BMS to ensure safe and high-performing operation of Li^+ batteries. This article demonstrated how the celebrated EKF

technique can be effectively applied to solve the SoC estimation problem and how fundamental concepts in nonlinear estimation theory can be readily utilized to enable the estimator design and interpret the estimation results.

This article performed a thorough observability and sensitivity analysis with a simple ECM battery model, which serves as a backbone for developing effective solutions to SoC estimation. An existing joint EKF-based adaptive SoC estimator, which performs simultaneous state and parameter estimation, is capable of producing accurate SoC estimation, albeit suffering from tuning difficulty and a relatively high computational cost. The tuning difficulty is in large due to fundamental limitations originating from the over-parametrized battery model and the limited data. Inspired by this analysis, this article further presented two custom-built EKFs, an enhanced EKF and a two-stage EKF, for adaptive SoC estimation. Compared with the joint EKF, the enhanced EKF enjoys advantages such as improved estimation accuracy, reduced tuning efforts, and a lower computational burden. The two-stage EKF shows comparable estimation performance but requires considerably less computation. Compared to the literature, this article builds the results on a systematic observability and sensitivity analysis, revealing and overcoming the potential pitfalls that can undermine a successful application of EKF to SoC estimation.

Despite the success of KF-based techniques in the SoC estimation, many questions remain open, which may represent opportunities for further investigation. First, how to prove the convergence properties of the SoC estimators? While there exist some results about the convergence of EKF, they have not been effectively transitioned to SoC estimation yet. Most nonlinear SoC observers also find themselves in a severe shortage of convergence analysis, because the battery models usually do not admit special structures often needed for relevant

proofs. Second, the full state estimation pursued in the existing works is indeed unnecessary as not every state or parameter will be of interest or use to the BMS, so how to construct reduced-order estimators or functional observers for higher computational accuracy? Third, going beyond the cell level, how to perform SoC monitoring and tracking for Li^+ battery packs? SoC estimation at the pack level is rendered more challenging and interesting by the increased system sophistication and mutual cell-to-cell influence. Along this line, an intriguing quest will be whether and how one can make the best use of the battery dynamics to reduce the number of voltage and current sensors without much sacrifice of estimation accuracy, please see Page 2.

References

[1] J.-M. Tarascon and M. Armand, "Issues and challenges facing rechargeable lithium batteries," *Nature*, vol. 414, pp. 359–367, Nov. 2001.

[2] M. Doyle, T. F. Fuller, and J. Newman, "Modeling of galvanostatic charge and discharge of the lithium/polymer/insertion cell," *J. Electrochem. Soc.*, vol. 140, no. 6, pp. 1526–1533, 1993.

[3] T. F. Fuller, M. Doyle, and J. Newman, "Simulation and optimization of the dual lithium ion insertion cell," *J. Electrochem. Soc.*, vol. 141, no. 1, pp. 1–10, 1994.

[4] C. Y. Wang, W. B. Gu, and B. Y. Liaw, "Micro-macrosopic coupled modeling of batteries and fuel cells I. model development," *J. Electrochem. Soc.*, vol. 145, no. 10, pp. 3407–3417, 1998.

[5] S. Atlung, K. West, and T. Jacobsen, "Dynamic aspects of solid solution cathodes for electrochemical power sources," *J. Electrochem. Soc.*, vol. 126, no. 8, pp. 1311–1321, 1979.

[6] S. Santhanagopalan, Q. Guo, P. Ramadass, and R. E. White, "Review of models for predicting the cycling performance of lithium ion batteries," *J. of Power Sources*, vol. 156, no. 2, pp. 620–628, 2006.

[7] N. Chaturvedi, R. Klein, J. Christensen, J. Ahmed, and A. Kojic, "Algorithms for advanced battery-management systems," *IEEE Contr. Sys. Mag.*, vol. 30, no. 3, pp. 49–68, 2010.

[8] S. K. Rahimian, S. Rayman, and R. E. White, "Extension of physics-based single particle model for higher charge-discharge rates," *J. of Power Sources*, vol. 224, pp. 180–194, 2013.

[9] G. L. Plett, "Extended Kalman filtering for battery management systems of LiPB-based

HEV battery packs: Part 2. modeling and identification," *J. of Power Sources*, vol. 134, no. 2, pp. 262–276, 2004.

[10] Y.-S. Lee and M.-W. Cheng, "Intelligent control battery equalization for series connected lithium-ion battery strings," *IEEE Trans. Ind. Electron.*, vol. 52, no. 5, pp. 1297–1307, Oct. 2005.

[11] M. Chen and G. A. Rincón-Mora, "Accurate electrical battery model capable of predicting runtime and I-V performance," *IEEE Trans. Energy Convers.*, vol. 31, no. 2, pp. 504–511, Jun. 2006.

[12] H. He, R. Xiong, and J. Fan, "Evaluation of lithium-ion battery equivalent circuit models for state of charge estimation by an experimental approach," *Energies*, vol. 4, pp. 582–598, 2011.

[13] Y. Hu, S. Li, and H. Peng, "A comparative study of equivalent circuit models for li-ion batteries," *J. of Power Sources*, vol. 198, pp. 359–367, Jan. 2012.

[14] R. Rao, S. Vrudhula, and D. N. Rakhmatov, "Battery modeling for energy-aware system design," *Computer*, vol. 36, no. 12, pp. 77–87, Dec. 2003.

[15] K. S. Narendra and A. M. Annaswamy, *Stable Adaptive Systems*. Englewood Cliffs, NJ: Prentice-Hall, 1989.

[16] T. Kim, Y. Wang, Z. Sahinoglu, T. Wada, and S. Hara, "Model-based condition monitoring for Lithium-Ion batteries," *J. of Power Sources*, vol. 295, pp. 16–27, Nov. 2015.

[17] H. Fang, Y. Wang, Z. Sahinoglu, T. Wada, and S. Hara, "Adaptive robust estimation of state of charge for lithium-ion batteries," in *Proc. 2013 ACC*, Washington, DC, 2013, pp. 3491–3497.

[18] R. Marino and P. Tomei, *Nonlinear Control Design: Geometric, Adaptive, and Robust*.

Hertfordshire, UK: Prentice-Hall, 1995.

[19] J. P. Gauthier, H. Hammouri, and S. Othman, "A simple observer for nonlinear systems–applications to bioreactors," *IEEE Trans. Automat. Control*, vol. 37, no. 6, pp. 875–880, Jun. 1992.

[20] J. P. Gauthier and I. A. K. Kupka, "Observability and observers for nonlinear systems," *SIAM J. Control Optim.*, vol. 32, no. 4, pp. 975–994, Jul. 1994.

[21] H. Nijmeijer and A. J. van der Schaft, *Nonlinear Dynamical Control Systems*. New York, NY: Springer, 1990.

[22] E. Busvelle and J. P. Gauthier, "High-gain and non-high-gain observers for nonlinear systems," *Contemporary Trends in Nonlinear Geometric Control Theory*, pp. 257–286, 2002.

[23] J. A. Farrell and M. Barth, *The Global Positioning System and Inertial Navigation*. New York: McGraw-Hill, 1998.

[24] R. Rajamani, "Observers for Lipschitz nonlinear systems," *IEEE Trans. Automat. Control*, vol. 43, no. 3, pp. 397–401, Mar. 1998.

[25] K. R. Shouse and D. G. Taylor, "Discrete-time observers for singularly perturbed continuous-time systems," *IEEE Trans. Automat. Control*, vol. 40, no. 2, pp. 224–235, Feb. 1995.

[26] G. H. Golun and C. F. V. Loan, *Matrix Computation*. Baltimore: JHU Press, 2012.

[27] J. P. Hespanha, D. Liberzon, D. Angeli, and E. D. Sontag, "Nonlinear norm-observability notations and stability of switched systems," *IEEE Trans. Automat. Control*, vol. 50, no. 2, pp. 154–168, Feb. 2005.

[28] A. J. Krener and A. Isidori, "Linearization by output injection and nonlinear observers,"

Syst. Control Lett., vol. 3, no. 1, pp. 47–52, Jun. 1983.

[29] A. J. Krener and W. Respondek, "Nonlinear observers with linearizable error dynamics," *SIAM J. Control Optim.*, vol. 23, no. 2, pp. 197–216, Mar. 1985.

[30] J. Rudolph and M. Zeitz, "Block triangular nonlinear observer normal form," *Syst. Control Lett.*, vol. 23, no. 1, pp. 1–8, Jul. 1994.

[31] W. Respondek, A. Pogromsky, and H. Nijmeijer, "Time scaling for observer design with linearizable error dynamics," *Automatica*, vol. 40, no. 2, pp. 277–285, Feb. 2004.

[32] Y. Wang and A. Lynch, "A block triangular observer forms for nonlinear observer design," *Int. J. Control*, vol. 81, no. 2, pp. 177–188, 2008.

[33] G. Zheng, D. Boutat, and J. Barbot, "Single output dependent observability normal form," *SIAM J. Control Optim.*, vol. 46, no. 6, pp. 2242–2255, 2007.

[34] W. Perruquetti, T. Floquet, and E. Moulav, "Finite-time observers: application to secure communication," *IEEE Trans. Automat. Control*, vol. 53, no. 2, pp. 356–360, Feb. 2008.

[35] J. H. Ahrens and H. K. Khalil, "High-gain observers in the presence of measurement noise: A switched-gain approach," *Automatica*, vol. 45, no. 4, pp. 936–943, Apr. 2009.

[36] Y. Wang and A. F. Lynch, "Multiple time scalings of a multi-output observer form," *IEEE Trans. Automat. Control*, vol. 55, no. 4, pp. 966–971, Apr. 2010.

[37] S. Julier, J. Uhlmann, and H. Durrant-Whyte, "A new approach for filtering nonlinear systems," in *Proceedings of American Control Conference*, vol. 3, 1995, pp. 1628–1632.

[38] S. J. Julier and J. K. Uhlmann, "A new extension of the Kalman filter to nonlinear systems," in *Proceedings of AeroSense: The 11th International Symposium on Aerospace/Defence Sensing, Simulation and Controls*, 1997, pp. 182–193.

[39] G. Evensen, "Sequential data assimilation with a nonlinear quasi-geostrophic model using

Monte Carlo methods to forecast error statistics," *Journal of Geophysical Research: Oceans*, vol. 99, no. C5, pp. 10 143–10 162, 1994.

[40] G. Evensen and P. J. van Leeuwen, "Assimilation of geosat altimeter data for the agulhas current using the ensemble Kalman filter with a quasigeostrophic model," *Monthly Weather Review*, vol. 124, pp. 85–96, 1996.

[41] P. L. Houtekamer and H. L. Mitchell, "Data assimilation using an ensemble Kalman filter technique," *Monthly Weather Review*, vol. 126, pp. 796–811, 1998.

[42] N. Gordon, D. Salmond, and A. Smith, "Novel approach to nonlinear/non-Gaussian Bayesian state estimation," *Radar and Signal Processing, IEE Proceedings F*, vol. 140, no. 2, pp. 107–113, 1993.

[43] C. Rao, J. Rawlings, and D. Mayne, "Constrained state estimation for nonlinear discrete-time systems: stability and moving horizon approximations," *IEEE Trans. Automat. Control*, vol. 48, no. 2, pp. 246–258, 2003.

[44] T. Wada, T. Takegami, and Y. Wang, "Sequential estimation of state of charge and equivalent circuit parameters for lithium-ion batteries," in *Proc. 2015 ACC*, Chicago, IL, Jul. 2015, pp. 2494–2498.

[45] A. B. Sripad and D. L. Snyder, "A necessary and sufficient condition for quantization errors to be uniform and white," *IEEE Transactions on Acoustics, Speech, and Signal Processing*, vol. ASSP-25, no. 5, pp. 442–448, Oct. 1977.

[46] B. Widrow, I. Kollár, and M.-C. Liu, "Statistical theory of quantization," *IEEE Transactions on Instrumentation and Measurement*, vol. 45, no. 2, pp. 353–351, Apr. 1996.

[47] M. Fu and C. E. de Souza, "State estimation for linear discrete-time systems using quantized measurements," *Automatica*, vol. 45, no. 12, pp. 2937–2945, Dec. 2009.

[48] Woodbank Communications Ltd, "Traction batteries for EV and HEV applications," http://www.mpoweruk.com/traction.htm.

[49] G. L. Plett, "Extended Kalman filtering for battery management systems of LiPB-based HEV battery packs: Part 3. state and parameter estimation," *J. of Power Sources*, vol. 134, no. 2, pp. 277–292, 2004.

[50] W. Ding, J. Wang, and C. Rizos, "Improving adaptive Kalman estimation in GPS/INS integration," *The Journal of Navigation*, vol. 60, pp. 517–529, 2007.

[51] F. V. Lima, M. R. Rajamanni, T. A. Soderstrom, and J. B. Rawlings, "Covariance and state estimation of weakly observable systems: application to polymerization processes," *IEEE Trans. Contr. Syst. Technol.*, vol. 21, no. 4, pp. 1249–1257, Jul. 2013.

[52] R. K. Mehra, "On the identification of variances and adaptive Kalman filtering," *IEEE Trans. Automat. Control*, vol. AC-15, no. 2, pp. 175–184, 1970.

[53] B. F. L. Scala, R. Bitmead, and B. G. Quinn, "An extended Kalman filter frequency tracker for high-noise environments," *IEEE Trans. Sig. Proc.*, vol. 44, no. 3, pp. 431–434, Feb. 1996.

[54] M. Boutayeb and D. Aubry, "A strong tracking extended Kalman observer for nonlinear discrete-time systems," *IEEE Trans. Automat. Control*, vol. 44, no. 8, pp. 1550–1556, Aug. 1999.

[55] J. Valappil and C. Georgakis, "Systematic estimation of the state noise statistics for extended Kalman filters," *AIChE J.*, vol. 46, no. 2, pp. 292–308, 2000.

[56] C.-S. Hsieh and F.-C. Chen, "Optimal solution of the two-stage kalman estimator," *IEEE Trans. Automat. Control*, vol. 44, no. 1, pp. 194–199, 1999.

[57] M. Hilairet, F. Auger, and E. Berthelot, "Speed and rotor flux estimation of induction

machines using a two-stage extended kalman filter," *Automatica*, vol. 45, no. 8, pp. 1819–1827, 2009.

[58] E. M. Tunali and T. J. Tarn, "New results for identifiability of nonlinear systems," *IEEE Trans. Automat. Control*, vol. AC-32, no. 2, pp. 146–154, Feb. 1987.

[59] X. Xia and C. H. Moog, "Identifiability of nonlinear systems with applications to HIV/AIDS models," *IEEE Trans. Automat. Control*, vol. 48, no. 2, pp. 330–336, Feb. 2003.

[60] A. Saltelli, M. Ratto, T. Andres, F. Campolongo, J. Cariboni, D. Gatelli, M. Saisana, and S. Tarantola, *Global Sensitivity Analysis: the Primer*. John Wiley & Sons, 2008.

[61] N. A. Noykova and M. Gyllenberg, "Sensitivity analysis and parameter estimation in a model of anaerobic waste water treatment processes with substrate inhibition," *Bioprocess Engineering*, vol. 23, no. 4, pp. 343–349, 2000.

[62] T. G. Müller, N. Noykova, M. Gyllenberg, and J. Timmer, "Practical identification in dynamical models of anerobic waste water treatment," *Mathematical Biosciences*, vol. 177, pp. 147–160, 2002.

[63] A. van Griensven, T. Meixner, S. Grunwald, T. Bishop, M. Diluzio, and R. Srinivasan, "A global sensivity analysis tool for the parameters of multi-variable catchment models," *Journal of Hybrology*, vol. 324, pp. 10–23, 2006.

[64] R. Brun, M. Kühni, H. Siegrist, W. Gujer, and P. Reichert, "Practical identifiability of ASM2d parameters-systematic selection and tuning of parameter subsets," *Water Research*, vol. 36, no. 16, pp. 4113–4127, 2002.

[65] M. Burth, G. C. Verghese, and M. Velez-Reyes, "Subset selection for improved parameter estimation in on-line identification of a synchronous generator," *IEEE Trans. Power Syst.*, vol. 14, no. 1, pp. 218–225, Feb. 1999.

[66] C. E. N. no and M. Velez-Reyes, "Dealing with ill conditioning in recursive parameter estimation for a synchronous generator," in *the 32nd Annual Conference of IEEE Industrial Electronics Society*, Paris, France, Nov. 2006, pp. 1089–1094.

[67] M. Boutayeb, H. Rafaralahy, and M. Darouach, "Convergence analysis of the extended Kalman filter used as an observer for nonlinear deterministic discrete-time systems," *IEEE Trans. Automat. Control*, vol. 42, no. 4, pp. 581–586, 1997.

[68] A. Krener, "The convergence of the extended Kalman filter," in *Directions in Mathematical Systems Theory and Optimization*, A. Rantzer and C. Byrnes, Eds. Springer, 2003, vol. 286, pp. 173–182.

[69] S. Kluge, K. Reif, and M. Brokate, "Stochastic stability of the extended Kalman filter with intermittent observations," *IEEE Trans. Automat. Control*, vol. 55, no. 2, pp. 514–518, 2010.

[70] S. Bonnabel and J.-J. Slotine, "A contraction theory-based analysis of the stability of the deterministic extended Kalman filter," *IEEE Trans. Automat. Control*, vol. 60, no. 2, pp. 565–569, 2015.

[71] H. Tanizaki, *Nonlinear Filters: Estimation and Applications*. Springer-Verlag Berlin Heidelberg, 1996.

[72] S. Särkkä, *Bayesian Filtering and Smoothing*. Cambridge University Press, 2013.

[73] M. Roth and F. Gustafsson, "An efficient implementation of the second order extended Kalman filter," in *Proceedings of the 14th International Conference on Information Fusion (FUSION)*, 2011, pp. 1–6.

[74] A. H. Jazwinski, *Stochastic processes and filtering theory*. New York, NY, USA: Academic Press, 1970.

[75] B. Bell and F. Cathey, "The iterated Kalman filter update as a gauss-newton method," *IEEE Trans. Automat. Control*, vol. 38, no. 2, pp. 294–297, 1993.

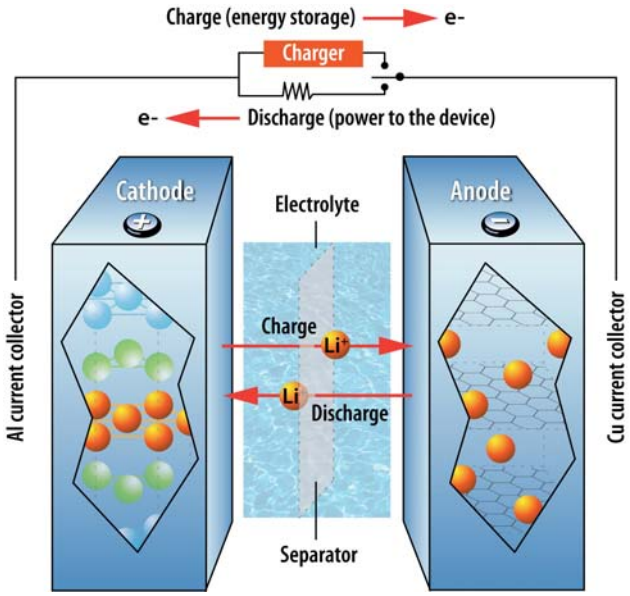

Figure 1. A schematic for the work mechanism of a Li^+ battery (source: Argonne National Laboratory). A Li^+ battery cell consists of four components: two electrodes including an anode and a cathode, the electrolyte, and an insulation separator. Both electrodes constitute small particles filled with active material. During charging or discharging, a reduction-oxidation reaction occurs at particles of one electrode and leads to release of Li^+ ions into the electrolyte; the Li^+ ions are transported to another electrode, where Li^+ ions are absorbed into particles.

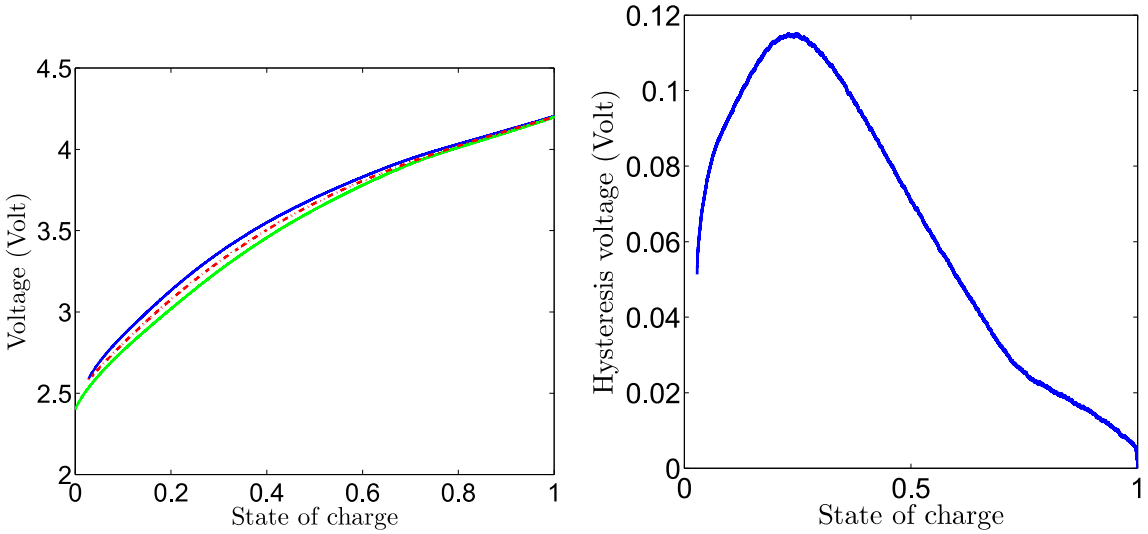

(a) (b)

Figure 2. The state of charge versus terminal voltage curves during discharge and charge processes. (a) terminal voltages while the battery is charged and discharged with a current 0.235A. Blue solid: the terminal voltage during the charge process (the charge curve); green solid: the terminal voltage during the discharge process (the discharge curve); red dash: the SoC-OCV curve obtained by averaging the discharge and charge curves. (b) the hysteresis between the charge and discharge curves. In the battery model (1), the hysteresis in the charge and discharge curves is captured by the series resistance, the RC circuit, and the hysteresis voltage x^3. Since the resistances are in the order of milliohm and the amplitude of currents is small, the voltages across the series resistor and the RC circuit are negligible, compared with x^3. The influence of temperature on the hysteresis is also suppressed by maintaining ambient temperature during the test. The SoC is obtained from the Coulomb counting method. The hysteresis voltage is SoC-dependent.

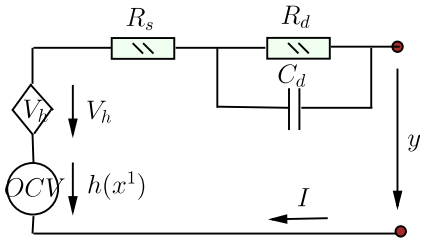

Figure 3. The equivalent circuit model corresponding to the battery model (1) consists of an RC circuit (R_d, C_d), a series resistor R_s, a hysteresis voltage source V_h, and a voltage source OCV. Both the hysteresis voltage and the OCV are SoC-dependent. The OCV is parameterized by a static function $h(x^1)$. $I > 0$ during discharge, and $I < 0$ during charge.

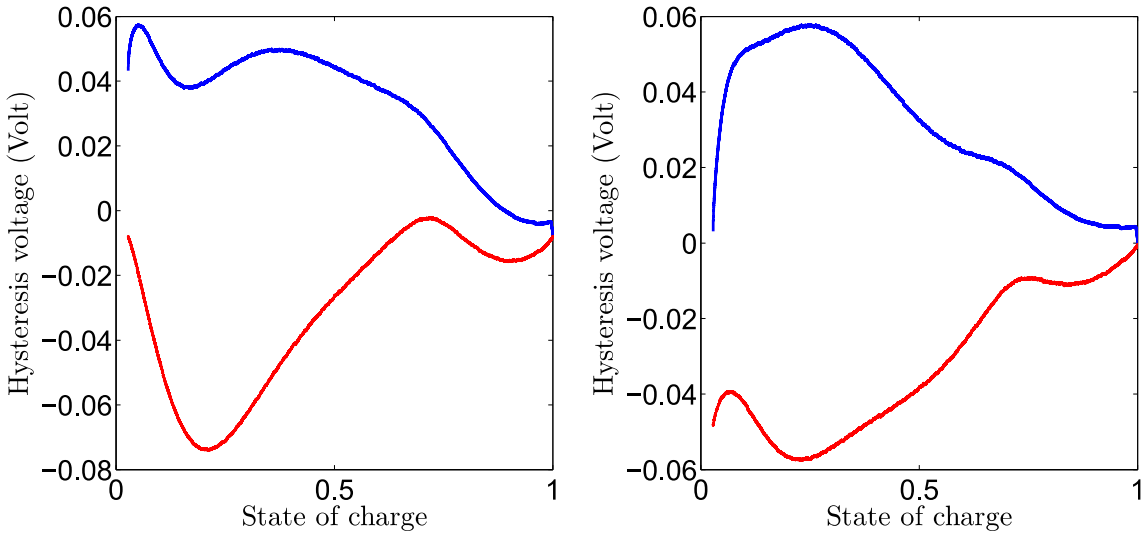

(a) (b)

Figure 4. The hysteresis voltage V_{hs} as a function of the SoC. Blue: the difference between the charge curve and the average curve predicted by different parameterizations of $h(x^1)$; red: the difference between the discharge curve and the average curve predicted by different parameterizations of $h(x^1)$. (a) V_{hs} with parametrization #1: $h(x^1) = a_0 \log(x^1 + a_1) + a_2$; (b) V_{hs} with parametrization #2: $h(x^1) = a_0 \exp(x^1) + a_1 + a_2 x^1 + a_3 (x^1)^2$.

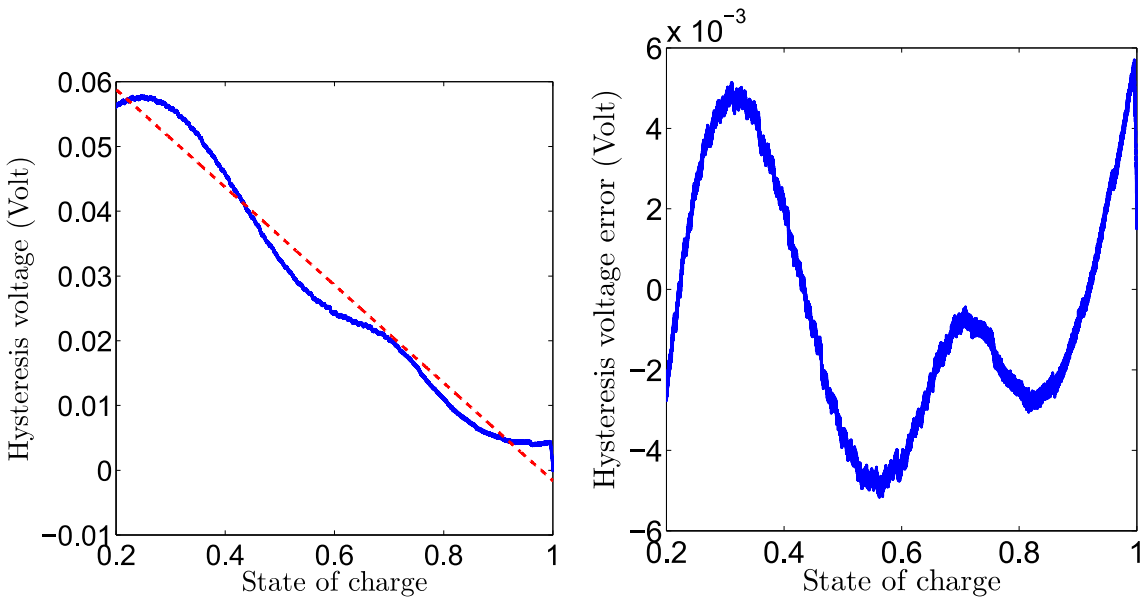

(a) (b)

Figure 5. The hysteresis voltage, its prediction, and the approximation error. (a) blue solid: the true hysteresis voltage V_{hs} (the difference between the charge curve and the average curve); the red dash: $\hat{V}_{hs}$ predicted by $(1-x^1)s$ with $s = 0.0755$. (b) the prediction error $V_{hs} - \hat{V}_{hs}$.

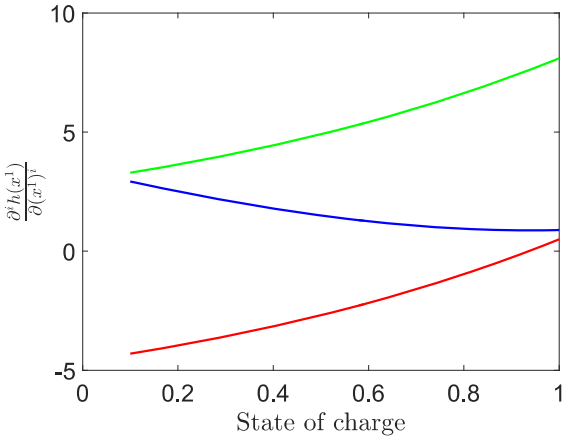

Figure 6. Derivatives of the open circuit voltage w.r.t. the state of charge. Blue: $\frac{\partial h(x^1)}{\partial x^1}$; red: $\frac{\partial^2 h(x^1)}{\partial (x^1)^2}$; green: $\frac{\partial^3 h(x^1)}{\partial (x^1)^3}$.

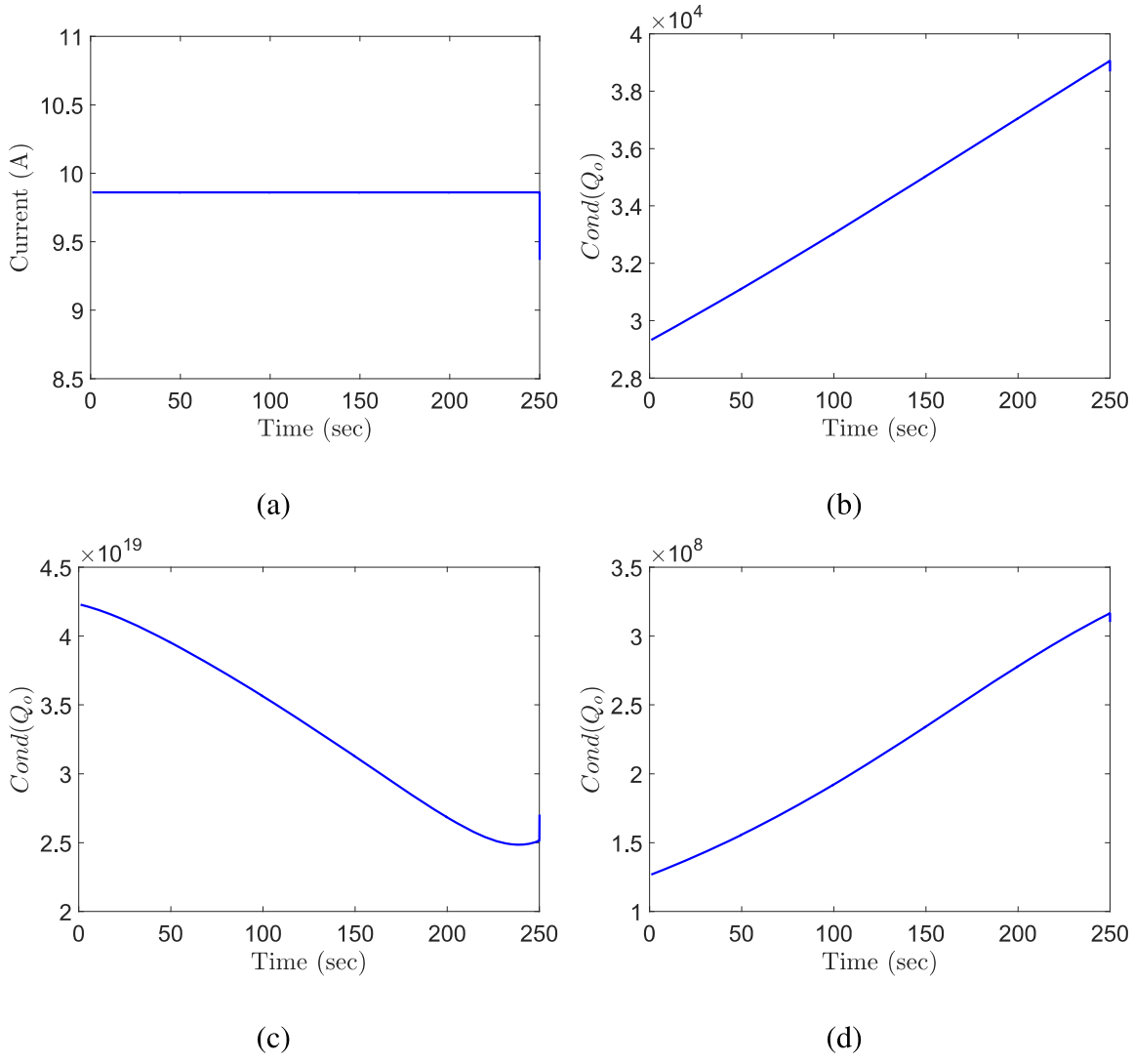

Figure 7. Condition numbers of the observability matrix Q_o when different battery models are subject to the constant current. (a) constant current. (b) the third order battery model (1). (c) the eighth order augmented battery model. (d) the fourth augmented battery model.

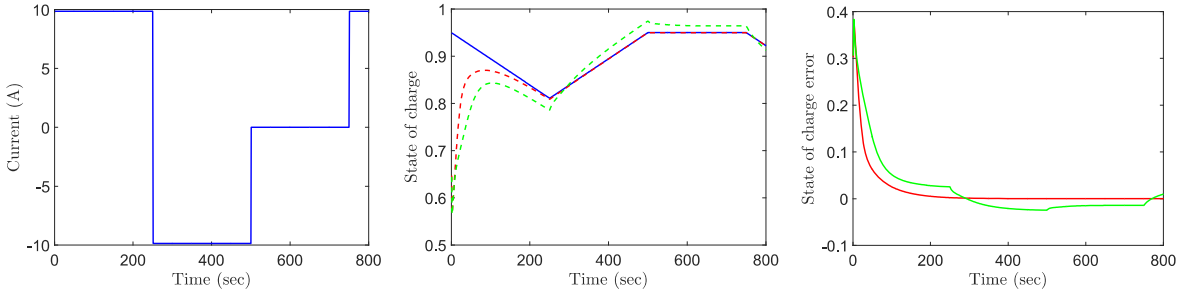

(a) (b) (c)

Figure 8. Validation of the EKF-based non-adaptive SoC estimator using synthetic data - pulse current case. (a) current. (b) blue solid: true SoC; red dash: SoC estimated by using true values of model parameters; green dash: SoC estimated where model parameters are 20% off true values. (c) red dash: SoC estimation error with true values of model parameters; green dash: SoC estimation error where model parameters are 20% off true values.

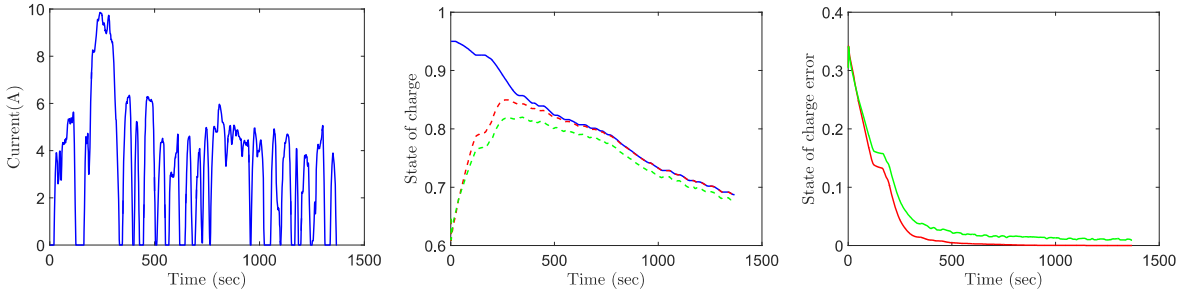

(a) (b) (c)

Figure 9. Validation of the EKF-based non-adaptive SoC estimator using synthetic data - UDDS current case. (a) current. (b) blue solid: true SoC; red dash: SoC estimated by using true values of model parameters; green dash: SoC estimated where model parameters are 20% off true values. (c) red dash: SoC estimation error with true values of model parameters; green dash: SoC estimation error where model parameters are 20% off true values.

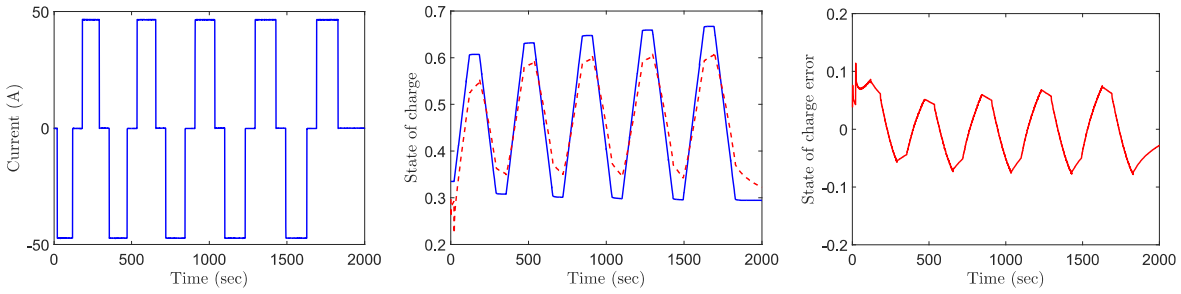

(a) (b) (c)

Figure 10. Validation of the EKF-based non-adaptive SoC estimator by experimental data. (a) current. (b) blue solid: true SoC from the Coulomb counting; red dash: estimated by the EKF. (c) the SoC estimation error.

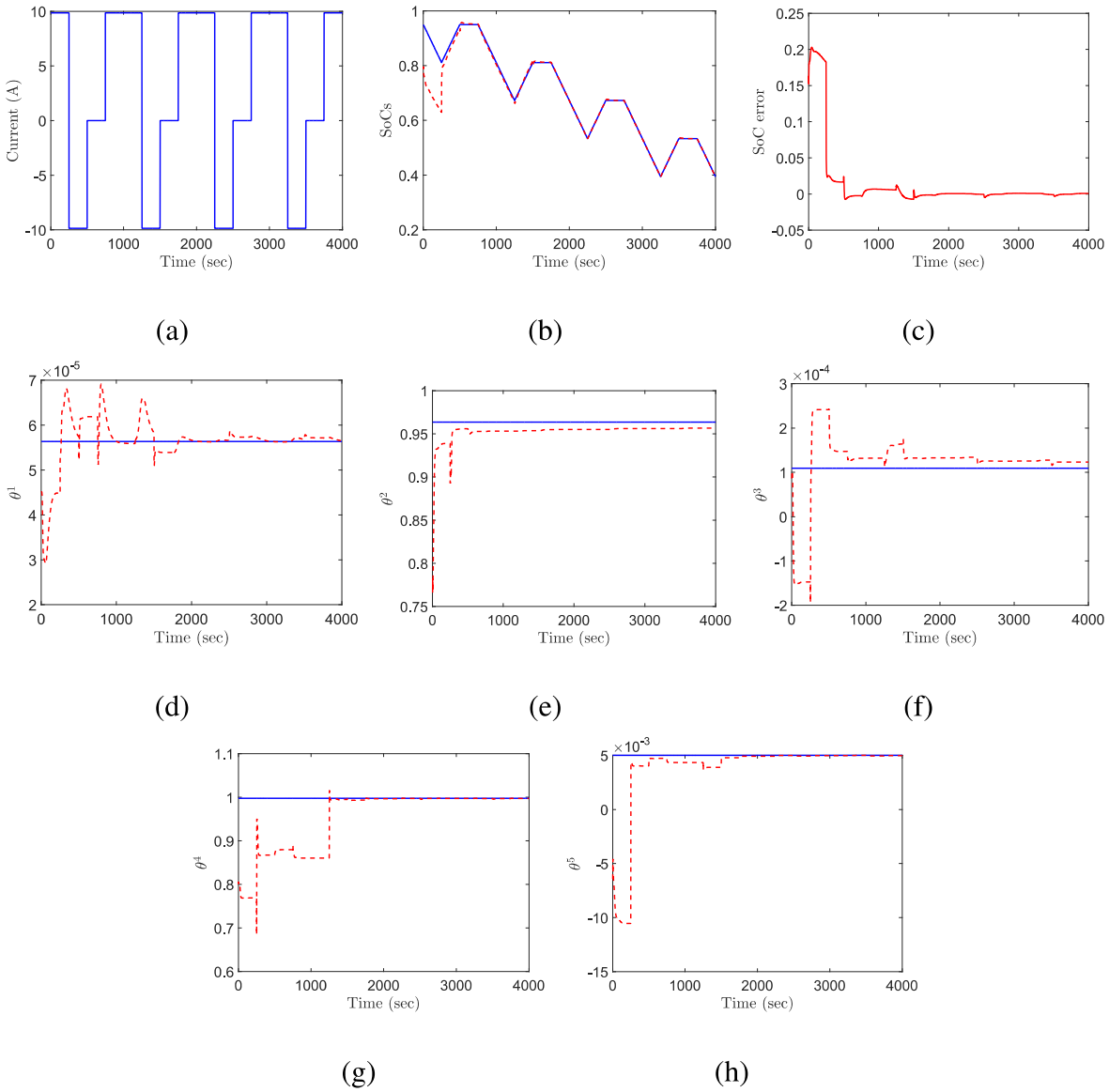

Figure 11. Validation of the joint EKF-based adaptive SoC estimator by synthetic data - pulse current case. (a) current (b) blue solid: true SoC; red dash: estimated. (c) SoC estimation error. (d) Blue solid: true θ^1; red dash: estimated. (e) Blue solid: true θ^2; red dash: estimated. (f) Blue solid: true θ^3; red dash: estimated. (g) Blue solid: true θ^4; red dash: estimated. (h) blue solid: true θ^5; red dash: estimated. Consistent with analysis results, tuning of the joint EKF is difficult to make the estimate of θ^2, θ^4 converge.

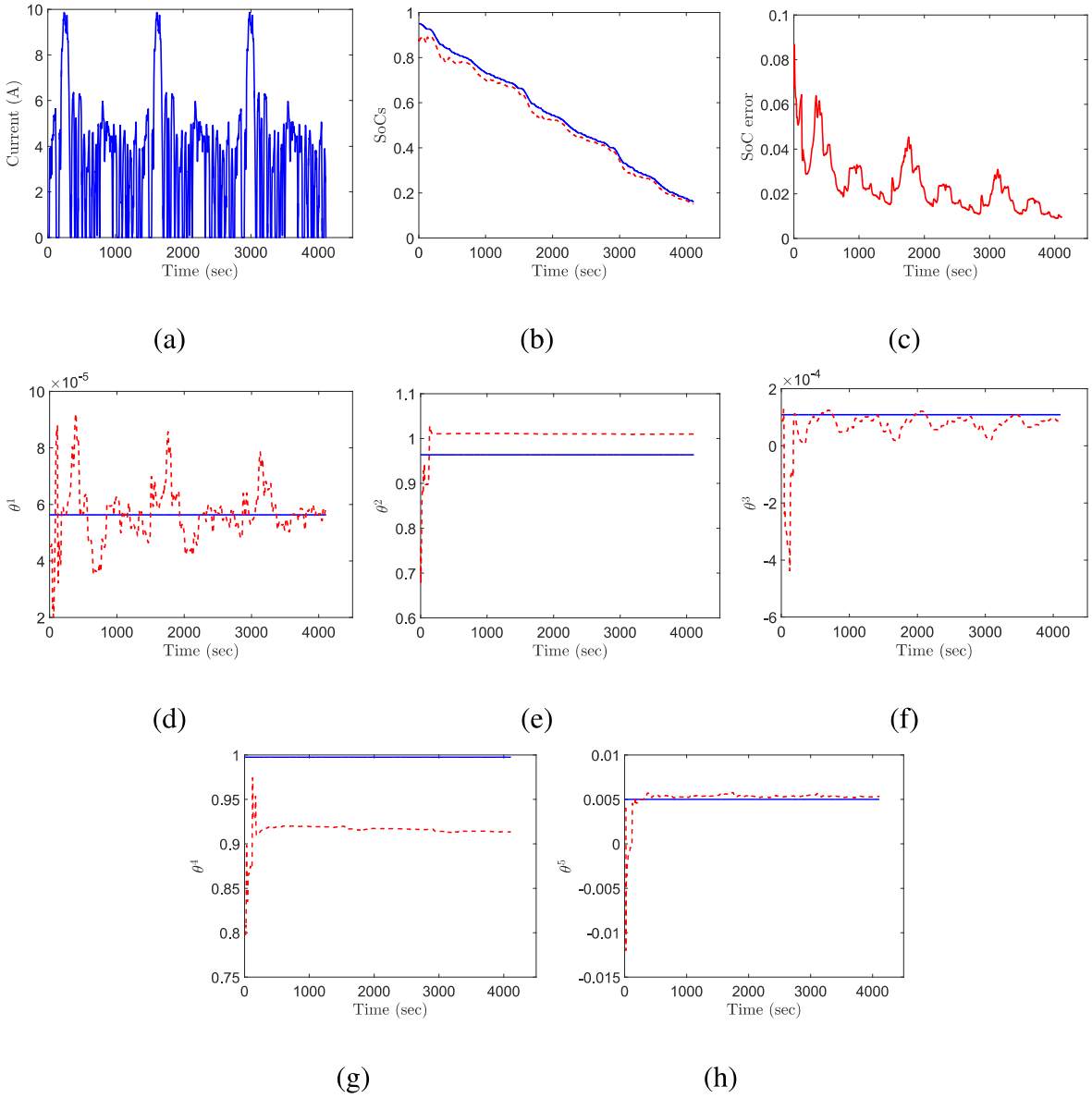

Figure 12. Validation of the joint EKF-based adaptive SoC estimator by synthetic data - UDDS current case. (a) current (b) blue solid: true SoC; red dash: estimated. (c) SoC estimation error. (d) Blue solid: true θ^1; red dash: estimated. (e) Blue solid: true θ^2; red dash: estimated. (f) Blue solid: true θ^3; red dash: estimated. (g) Blue solid: true θ^4; red dash: estimated. (h) blue solid: true θ^5; red dash: estimated. Consistent with analysis results, tuning of the joint EKF is difficult to make the estimate of θ^2, θ^4 converge.

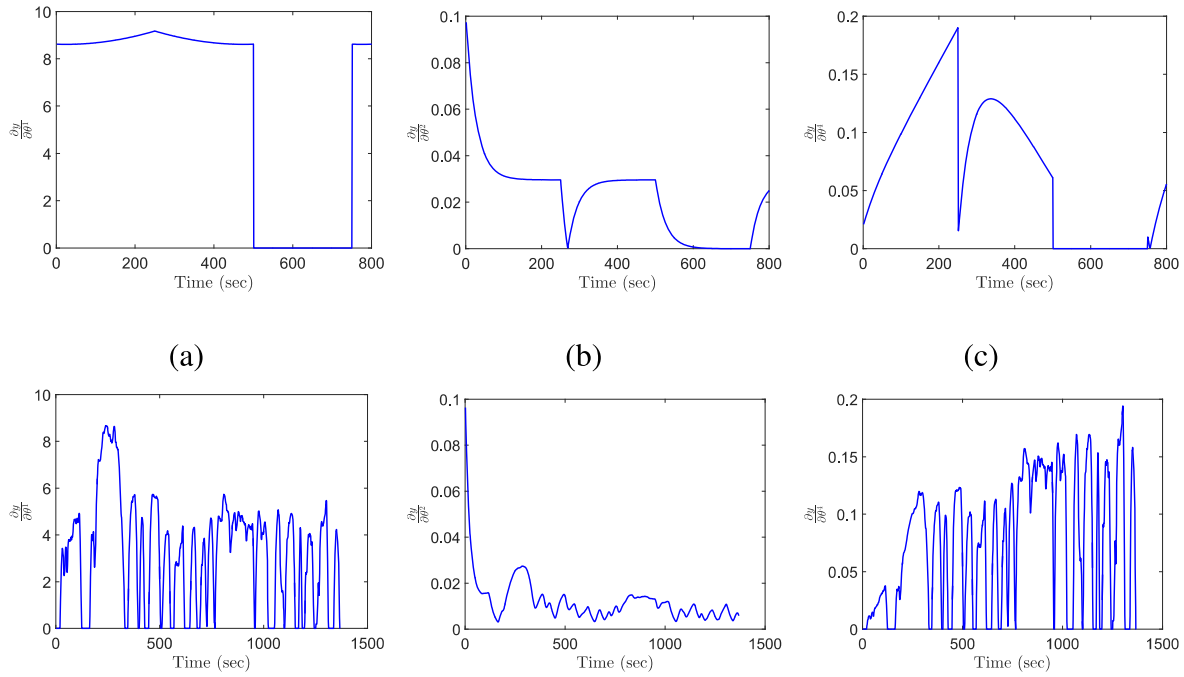

(a) (b) (c)

(d) (e) (f)

Figure 13. Simulation results of sensitivity analysis: $\partial y/\partial \theta^1$, $\partial y/\partial \theta^2$, and $\partial y/\partial \theta^4$ when the battery model (1) is subject to the pulse current and the UDDS current, respectively. (a)-(c): pulse current; (d)-(f): UDDS current. (a) $\partial y/\partial \theta^1$. (b) $\partial y/\partial \theta^2$. (c) $\partial y/\partial \theta^4$. (d) $\partial y/\partial \theta^1$. (e) $\partial y/\partial \theta^2$. (f) $\partial y/\partial \theta^4$.

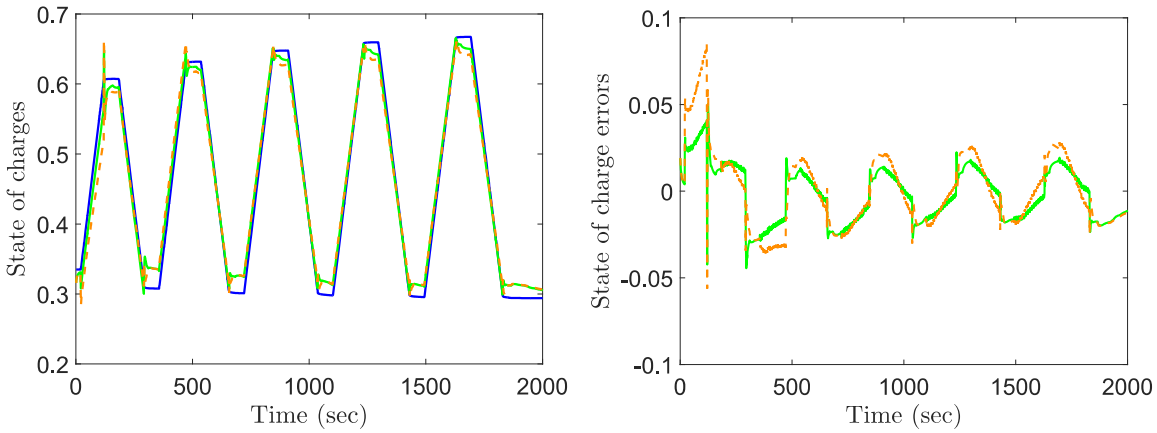

(a) (b)

Figure 14. Comparison of the two-stage EKF and the joint EKF using experimental data. (a) blue solid: true SoC from the Coulomb counting; green solid: joint EKF; orange dash: two-stage EKF. (b) the SoC estimation error; green solid: joint EKF; orange dash: two-stage EKF.

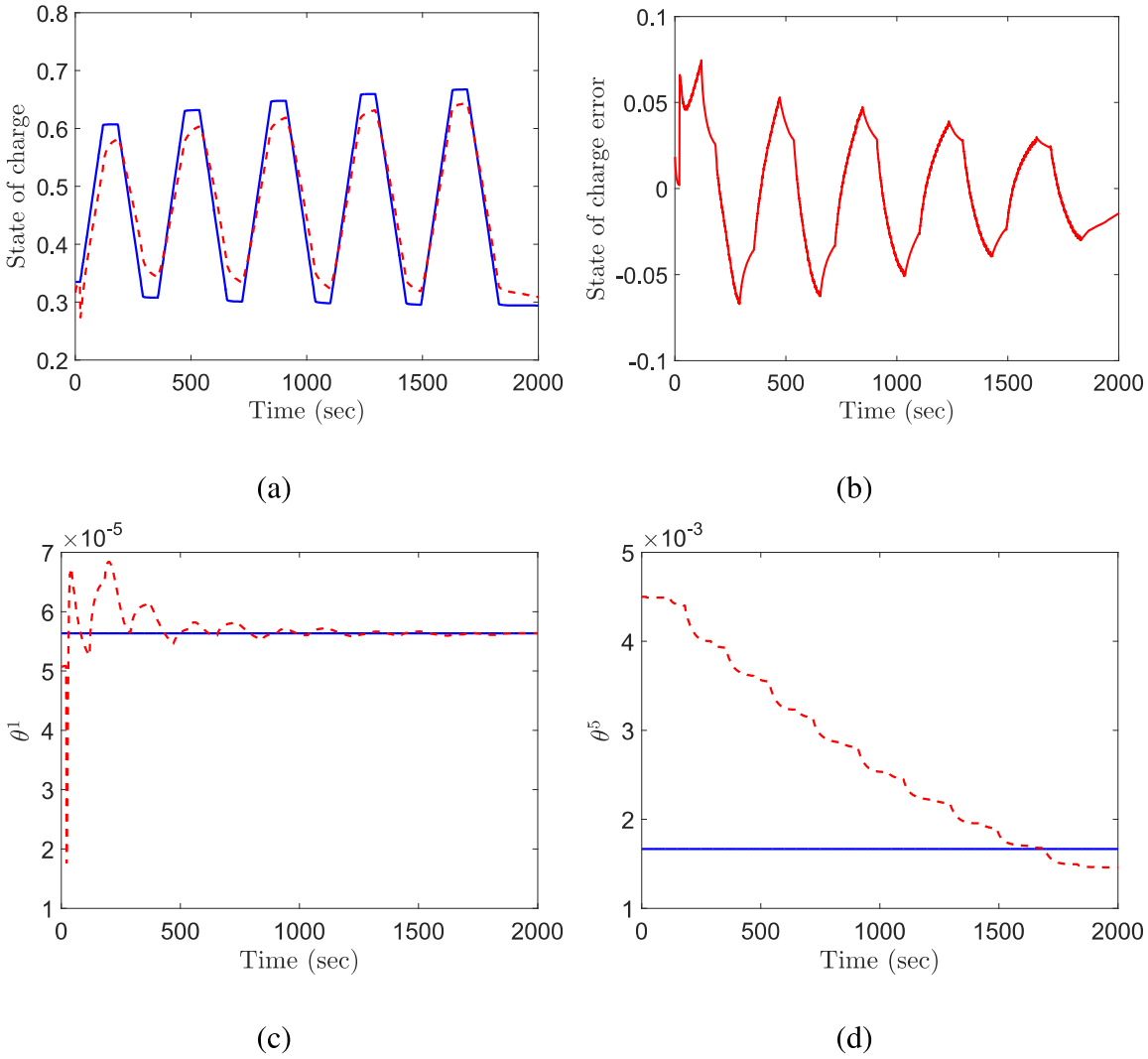

Figure 15. Validation of the EKF-A using experimental data. (a) blue: true SoC from the Coulomb counting; red dash: estimated. (b) the SoC estimation error. (c) blue: nominal θ^1; red dash: estimated. (d) blue: nominal θ^5; red dash: estimated.

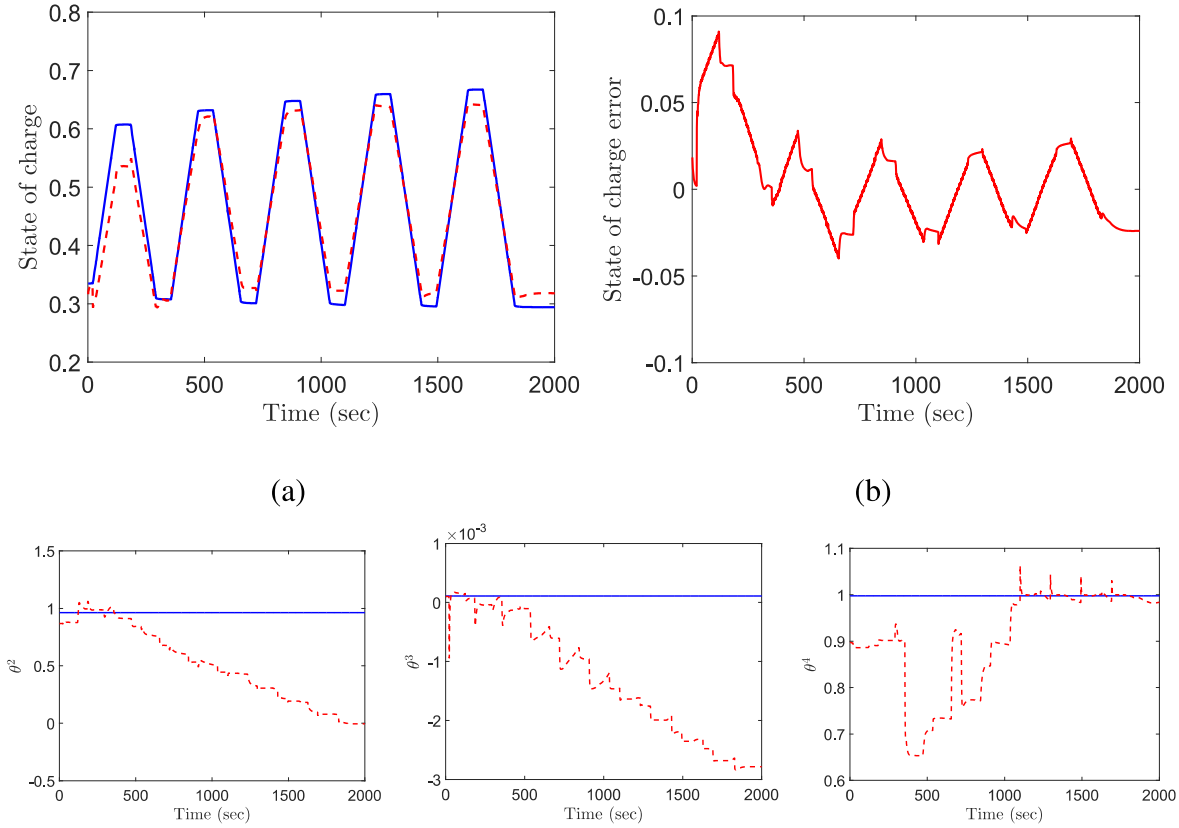

Figure 16. Validation of the EKF-B using experimental data. (a) blue: true SoC from the Coulomb counting; red dash: estimated. (b) the SoC estimation error. (c) blue: nominal θ^2; red dash: estimated. (d) blue: nominal θ^3; red dash: estimated θ^3. (e) blue: nominal θ^4; red dash: estimated θ^4.

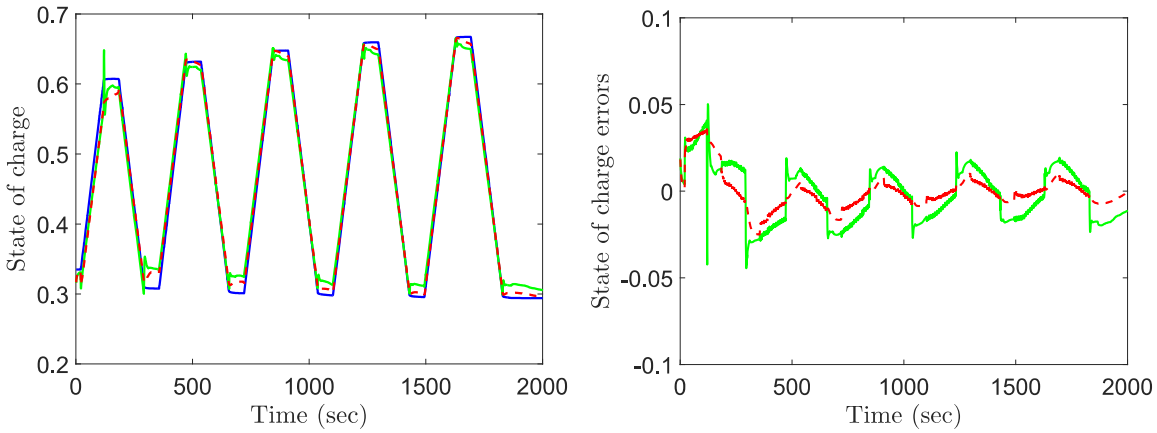

(a) (b)

Figure 17. Comparison of the enhanced EKF and the joint EKF using experimental data. (a) blue: true SoC from the Coulomb counting; green: joint EKF; red dash: enhanced EKF. (b) the SoC estimation error; green: joint EKF; red dash: enhanced EKF.

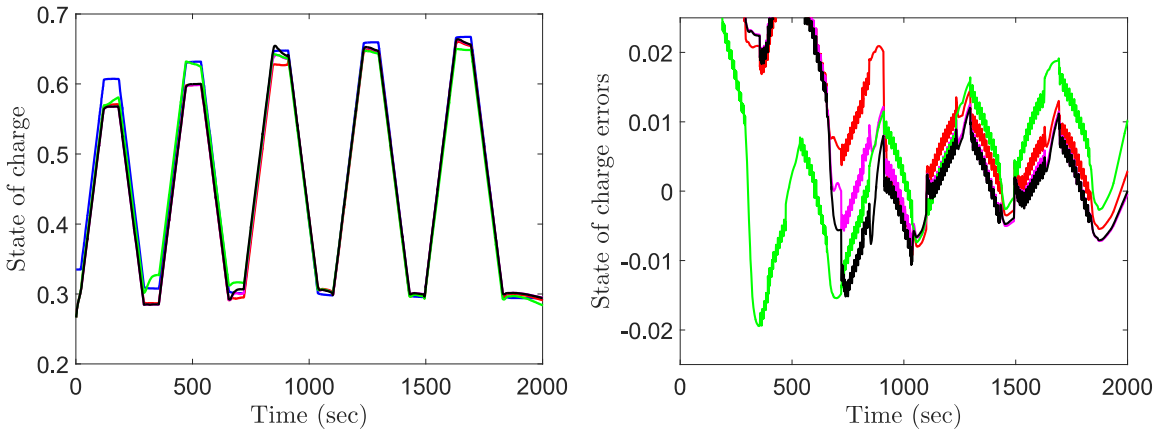

(a) (b)

Figure 18. Robustness of the enhanced EKF with different Q and R, and experimental data. Red: Q,R take nominal values; magenta: Q,R are 10 times larger; black: Q,R are 100 times larger; green: Q,R are one tenth of nominal values; (a) SoC estimates. (b) SoC estimation errors.

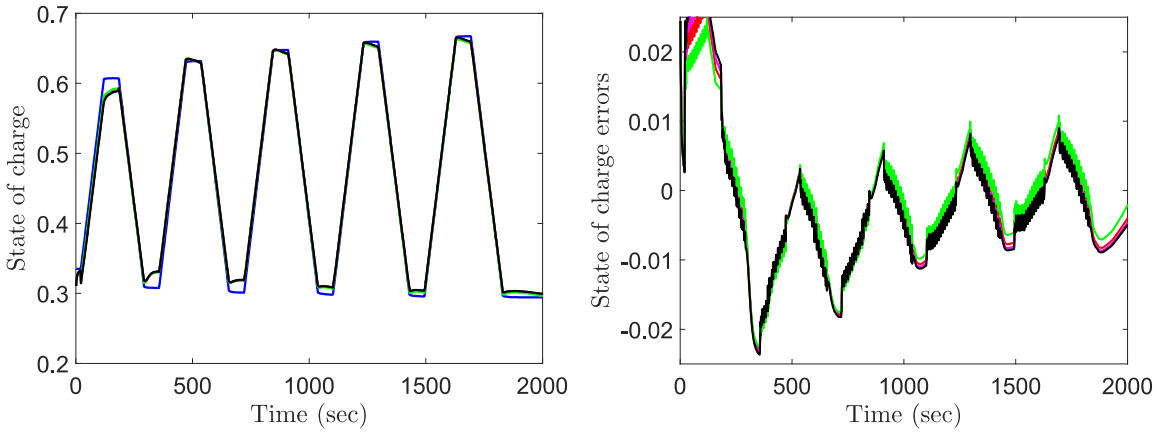

(a) (b)

Figure 19. Robustness of the enhanced EKF with different $q^4,\ldots,q^8$, and experimental data. Red: $q^4,\ldots,q^8$ takes nominal values; magenta: $q^4,\ldots,q^8$ are 1.5 times larger; black: $q^4,\ldots,q^8$ are 2 times larger; green: $q^4,\ldots,q^8$ are half of nominal values; (a) SoC estimates. (b) SoC estimation errors.

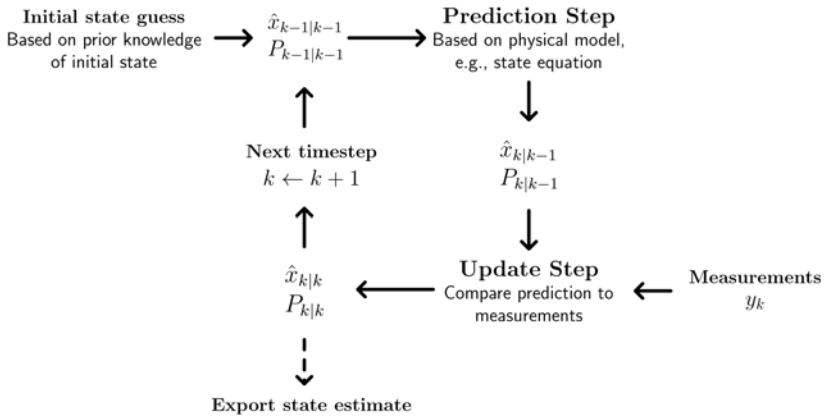

Figure S1. A schematic of the EKF structure, modified from [S52]. The EKF comprises two steps sequentially executed through time, prediction and update. For prediction, one looks to x_k at time $k-1$ and predicts x_k. The forecast is denoted as $\hat{x}_{k|k-1}$ and subject to uncertainty quantified by the prediction error covariance $P_{k|k-1}$. The update step occurs upon the arrival of the new measurement y_k. In this step, y_k is leveraged to correct $\hat{x}_{k|k-1}$ and produce the updated estimate $\hat{x}_{k|k}$. Meanwhile, $P_{k|k-1}$ is updated to generate $P_{k|k}$ to quantify the uncertainty imposed on $\hat{x}_{k|k}$.

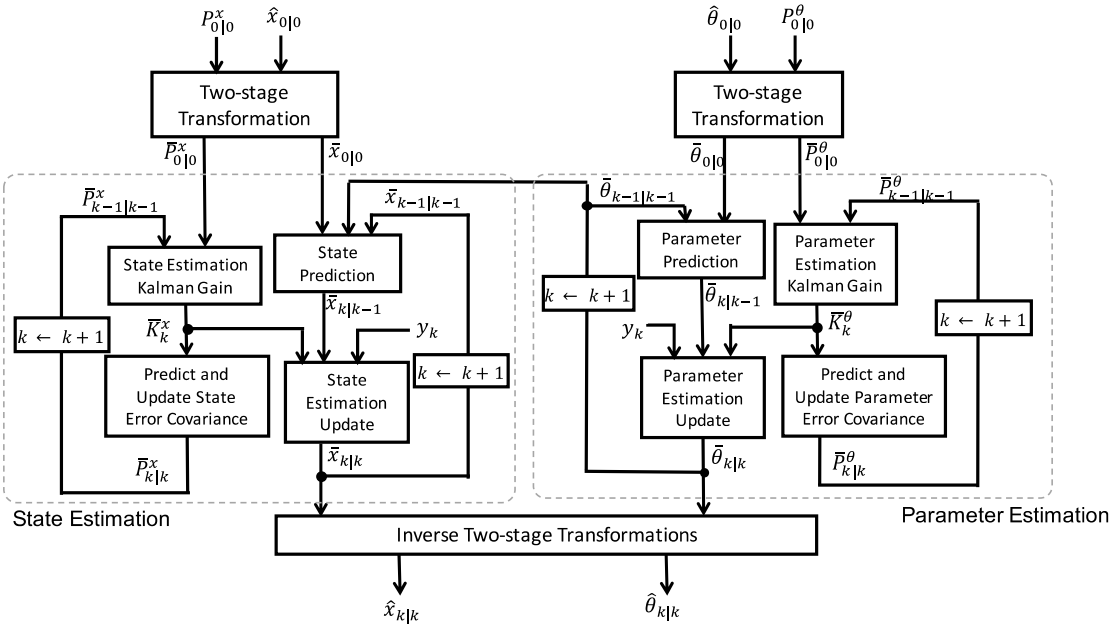

Figure S2. Two-stage EKF block diagram.

Sidebar 1: A Survey of State of Charge Estimation

Li^+ batteries are widely recognized as a key enabler for the worldwide migration toward clean and sustainable energy supply, with tremendous application in the sectors of transportation, aerospace, buildings, renewables and smart grid. Due to the materials used and the electrochemistries, they, however, are vulnerable to overcharging and overdischarging, which can cause fast aging and even trigger fire and explosion in extreme cases. An accurate SoC estimation thus becomes a necessity to avoid such issues and furthermore, provide a foundation of support for other higher-level battery management tasks. Depending on the explicit use of a battery model or not, the existing SoC estimation methods can be divided into two categories, *non-model-based* and *model-based*, an update-to-date review of which is offered below.

Conventional model-free methods are based on measuring or calculating certain parameters directly linked with the SoC. Two straightforward yet representative methods in this regard are voltage translation and Coulomb counting [S1]. The former infers the SoC from the predetermined OCV-SoC lookup table using the OCV measurement. Despite the reliability, it requires the battery to rest for a long period with cutting off from the external circuit in order to measure the OCV. Coulomb counting is based on numerical integration of the current over time. It is easy to implement but can suffer from a 'drift' from the true values due to cumulative integration errors and noise corruption. These methods have still gained much popularity because of their simplicity and convenience. They are also integrated with model-based methods in some recent developments for improved SoC estimation, see [S2], [S3]. Another class of model-free SoC estimation methods are based on machine learning. Without requiring an equivalent-circuit or electrochemical model, they train the battery data sets to build an abstract

mathematical description to approximate the battery behavior and then estimate the SoC. The main tools that have been investigated include artificial neural networks [S4]–[S7] and support vector machine [S8]–[S11]. With sights set on data-driven inference and reasoning, machine learning offers a useful means of mining the battery operation data collected through time for SoC monitoring and more tasks. The training, however, can be complex and may imply much preparatory work before the algorithm deployment. In addition, the neural-network computation can be costly and thus unsuitable for onboard application.

Given the availability of a diverse range of battery models, recent years have seen a shift of attention toward model-based SoC estimation methods, which can promise improved accuracy while allowing real-time execution. This research front, at the nexus of Li^+ battery systems and estimation theory, is expanding rapidly, with a large body of work published. Results based on both equivalent-circuit and electrochemical models have been widely reported. The equivalent-circuit-based models generally offers a low-complexity description of the Li^+ battery dynamics with fewer states and parameters, thus conducive to fast SoC estimation. The electrochemical models, in the form of PDEs, represent a more sophisticated view of the battery dynamics while often requiring more computational or model reduction effort. From the perspective of estimation, the existing literature puts two types of approaches into use, namely, *stochastic estimation* and *nonlinear observer*. For the former type, the KF is in a leading position. Many KF techniques, including EKF, iterated EKF, and sigma-point KF, have been applied to different SoC problem settings or battery models [S12]–[S19], [S19]–[S29]. Another avenue builds on particle filtering (PF), which is capable of handling severe nonlinearities and non-Gaussian noise and has led to a few research works [S30]–[S33]. The stochastic estimation approach has emerged as a natural choice primarily for its ability to suppress the noise affecting a battery system. Its appeal is

further enhanced by the applicability to general nonlinear systems and thus almost every battery model, working to the advantage of the developer. When it comes to computational efficiency, the KFs are competitive, especially when used for a low-dimensional battery model, as needed to be successful with real-world implementation, and the PFs, by contrast, will demand more computational resources. Although the convergence properties of these methods are difficult to analyze due to nonlinearities and noise, the above merits have still made them among the most favored choices in practice. The second type of model-based methods, called nonlinear SoC observers, have also drawn much interest in the past several years. The present literature now covers a broad range of design techniques, including Luenberger observer [S1], [S34], adaptive observer [S35]–[S40], sliding mode observer [S41]–[S44], output-injection PDE observer [S45]–[S47], backstepping PDE observer [S48], and robust nonlinear observer [S49]. The SoC observers proceed on the premise that the battery system is at least approximately deterministic. Though restrictive to some extent, the deterministic assumption eliminates the need for maintaining covariance matrices and thus enables higher efficiency of SoC estimation. The observer approach, while enjoying application to equivalent-circuit models, is also suitable for some PDE-based battery models such as the SPM.

References

[S1] C. D. Rahn and C.-Y. Wang, *Battery Management Systems*. John Wiley & Sons Ltd, 2013, pp. 191–229.

[S2] F. Codeca, S. M. Savaresi, and G. Rizzoni, “On battery state of charge estimation: A new mixed algorithm,” in *Proceedings of IEEE International Conference on Control*

Applications, 2008, pp. 102–107.

[S3] M. Verbrugge and E. Tate, "Adaptive state of charge algorithm for nickel metal hydride batteries including hysteresis phenomena," *Journal of Power Sources*, vol. 126, no. 1, pp. 236 – 249, 2004.

[S4] M. Charkhgard and M. Farrokhi, "State-of-charge estimation for lithium-ion batteries using neural networks and EKF," *IEEE Transactions on Industrial Electronics*, vol. 57, no. 12, pp. 4178–4187, 2010.

[S5] C.-H. Cai, Dong-Du, Z.-Y. Liu, and H. Zhang, "Artificial neural network in estimation of battery state of-charge (soc) with nonconventional input variables selected by correlation analysis," in *Proceedings of International Conference on Machine Learning and Cybernetics*, vol. 3, 2002, pp. 1619–1625.

[S6] A. Affanni, A. Bellini, C. Concari, G. Franceschini, E. Lorenzani, and C. Tassoni, "Ev battery state of charge: neural network based estimation," in *Proceedings of IEEE International Electric Machines and Drives Conference*, vol. 2, 2003, pp. 684–688.

[S7] G. W. W. L. Bi Jun, Shao Sai, "State of charge estimation of li-ion batteries in electric vehicle based on radial-basis-function neural network," *Chinese Physics B*, vol. 21, no. 11, p. 118801, 2012.

[S8] J. Hu, J. Hu, H. Lin, X. Li, C. Jiang, X. Qiu, and W. Li, "State-of-charge estimation for battery management system using optimized support vector machine for regression," *Journal of Power Sources*, vol. 269, pp. 682 – 693, 2014.

[S9] J. C. A. Anton, P. J. G. Nieto, C. B. Viejo, and J. A. V. Vilan, "Support vector machines used to estimate the battery state of charge," *IEEE Transactions on Power Electronics*, vol. 28, no. 12, pp. 5919–5926, 2013.

[S10] Q. S. Shi, C. H. Zhang, and N. X. Cui, "Estimation of battery state-of-charge using v-support vector regression algorithm," *International Journal of Automotive Technology*, vol. 9, no. 6, pp. 759–764, 2008.

[S11] "Support vector based battery state of charge estimator," *Journal of Power Sources*, vol. 141, no. 2, pp. 351 – 358, 2005.

[S12] D. Di Domenico, A. Stefanopoulou, and G. Fiengo, "Lithium-ion battery state of charge and critical surface charge estimation using an electrochemical model-based extended Kalman filter," vol. 132, no. 6, 2010.

[S13] H. Fang, Y. Wang, Z. Sahinoglu, T. Wada, and S. Hara, "State of charge estimation for lithium-ion batteries: An adaptive approach," *Control Engineering Practice*, vol. 25, pp. 45 – 54, 2014.

[S14] H. Fang, X. Zhao, Y. Wang, Z. Sahinoglu, T. Wada, S. Hara, and R. A. de Callafon, "Improved adaptive state-of-charge estimation for batteries using a multi-model approach," *Journal of Power Sources*, vol. 254, pp. 258 – 267, 2014.

[S15] H. Fang, Y. Wang, Z. Sahinoglu, T. Wada, and S. Hara, "Adaptive estimation of state of charge for lithium-ion batteries," in *Proceedings of American Control Conference*, 2013, pp. 3485–3491.

[S16] Y. Zou, X. Hu, H. Ma, and S. E. Li, "Combined state of charge and state of health estimation over lithium-ion battery cell cycle lifespan for electric vehicles," *Journal of Power Sources*, vol. 273, pp. 793–803, 2015.

[S17] J. Lee, O. Nam, and B. Cho, "Li-ion battery SOC estimation method based on the reduced order extended Kalman filtering," *Journal of Power Sources*, vol. 174, no. 1, pp. 9–15, 2007.

[S18] J. Han, D. Kim, and M. Sunwoo, "State-of-charge estimation of lead-acid batteries using

an adaptive extended Kalman filter," *Journal of Power Sources*, vol. 188, no. 2, pp. 606–612, 2009.

[S19] O. Barbarisi, F. Vasca, and L. Glielmo, "State of charge Kalman filter estimator for automotive batteries," *Control Engineering Practice*, vol. 14, no. 3, pp. 267–275, 2006.

[S20] S. Santhanagopalan and R. E. White, "State of charge estimation using an unscented filter for high power lithium ion cells," *International Journal of Energy Research*, vol. 34, no. 2, pp. 152–163, 2010.

[S21] G. L. Plett, "Sigma-point Kalman filtering for battery management systems of LiPB-based HEV battery packs: Part 2: Simultaneous state and parameter estimation," *Journal of Power Sources*, vol. 161, no. 2, pp. 1369–1384, 2006.

[S22] S. Pang, J. Farrell, D. J., and M. Barth, "Battery state-of-charge estimation," in *Proceedings of American Control Conference*, vol. 2, 2001.

[S23] C. Weng, J. Sun, and H. Peng, "A unified open-circuit-voltage model of lithium-ion batteries for state-of-charge estimation and state-of-health monitoring," *Journal of Power Sources*, vol. 258, pp. 228–237, 2014.

[S24] "Model-based electrochemical estimation and constraint management for pulse operation of lithium ion batteries," *IEEE Transactions on Control Systems Technology*, vol. 18, no. 3.

[S25] R. Xiong, X. Gong, C. C. Mi, and F. Sun, "A robust state-of-charge estimator for multiple types of lithium-ion batteries using adaptive extended Kalman filter," *Journal of Power Sources*, vol. 243, pp. 805–816, 2013.

[S26] A. Bizeray, S. Zhao, S. Duncan, and D. Howey, "Lithium-ion battery thermal-electrochemical model-based state estimation using orthogonal collocation and a modified extended Kalman filter," *Journal of Power Sources*, vol. 296, pp. 400–412, 2015.

[S27] C. Taborelli and S. Onori, "State of charge estimation using extended kalman filters for battery management system," in *IEEE International Electric Vehicle Conference*, 2014, pp. 1–8.

[S28] X. Lin, A. Stefanopoulou, P. Laskowsky, J. Freudenberg, Y. Li, and R. Dyche, "State of charge estimation error due to parameter mismatch in a generalized explicit lithium ion battery model," in *Proceedings of ASME Dynamic Systems and Controls Conference*, 2011, pp. 393–400.

[S29] T. Kim, Y. Wang, H. Fang, Z. Sahinoglu, T. Wada, S. Hara, and W. Qiao, "Model-based condition monitoring for lithium-ion batteries," *Journal of Power Sources*, vol. 295, pp. 16–27, 2015.

[S30] A. Bartlett, J. Marcicki, S. Onori, G. Rizzoni, X. G. Yang, and T. Miller, "Electrochemical model-based state of charge and capacity estimation for a composite electrode lithium-ion battery," *IEEE Transactions on Control Systems Technology*, vol. 24, no. 2, pp. 384–399, 2016.

[S31] Y. Wang, C. Zhang, and Z. Chen, "A method for state-of-charge estimation of LiFePO4 batteries at dynamic currents and temperatures using particle filter," *Journal of Power Sources*, vol. 279, pp. 306–311, 2015.

[S32] M. F. Samadi, S. M. M. Alavi, and M. Saif, "Online state and parameter estimation of the li-ion battery in a bayesian framework," in *Proceedings of American Control Conference*, 2013, pp. 4693–4698.

[S33] R. Restaino and W. Zamboni, "Comparing particle filter and extended Kalman filter for battery state-of-charge estimation," in *Proceedings of 38th Annual Conference on IEEE Industrial Electronics Society*, 2012, pp. 4018–4023.

[S34] Q. Ouyang, J. Chen, F. Wang, and H. Su, "Nonlinear observer design for the state of charge of lithium-ion batteries," in *Proceedings of 9th World Congress The International Federation of Automatic Control*, 2014, pp. 2794–2799.

[S35] Y. Wang, H. Fang, Z. Sahinoglu, T. Wada, and S. Hara, "Adaptive estimation of the state of charge for lithium-ion batteries: Nonlinear geometric observer approach," *IEEE Transactions on Control Systems Technology*, 2015, in press.

[S36] ——, "Nonlinear adaptive estimation of the state of charge for lithium-ion batteries," in *Proceedings of IEEE Conference on Decision & Control*, 2013, pp. 4405–4410.

[S37] M. El Lakkis, O. Sename, M. Corno, and D. Bresch Pietri, "Combined battery soc/soh estimation using a nonlinear adaptive observer," in *Proceedings of European Control Conference*, 2015, pp. 1522–1527.

[S38] L. Liu, L. Y. Wang, Z. Chen, C. Wang, F. Lin, and H. Wang, "Integrated system identification and state-of-charge estimation of battery systems," *IEEE Transactions on Energy Conversion*, vol. 28, no. 1, pp. 12–23, 2013.

[S39] S. Dey, B. Ayalew, and P. Pisu, "Nonlinear adaptive observer for a lithium-ion battery cell based on coupled electrochemical-Thermal model," vol. 137, no. 11, 2014.

[S40] Y. Li, R. D. Anderson, J. Song, A. M. Phillips, and X. Wang, "A nonlinear adaptive observer approach for state of charge estimation of lithium-ion batteries," in *Proceedings of the 2011 American Control Conference*, 2011, pp. 370–375.

[S41] I.-S. Kim, "The novel state of charge estimation method for lithium battery using sliding mode observer," *Journal of Power Sources*, vol. 163, no. 1, pp. 584–590, 2006.

[S42] A. Belhani, N. K. M'Sirdi, and A. Naamane, "Adaptive sliding mode observer for estimation of state of charge," *Energy Procedia*, vol. 42, pp. 377 – 386, 2013.

[S43] X. Chen, W. Shen, Z. Cao, A. Kapoor, and I. Hijazin, "Adaptive gain sliding mode observer for state of charge estimation based on combined battery equivalent circuit model in electric vehicles," in *Proceedings of IEEE 8th Conference on Industrial Electronics and Applications*, 2013, pp. 601–606.

[S44] F. Zhang, G. Liu, and L. Fang, "A battery state of charge estimation method using sliding mode observer," in *Proceedings of 7th World Congress on Intelligent Control and Automation*, 2008, pp. 989–994.

[S45] S. J. Moura, N. A. Chaturvedi, and M. Krstic, "Pde estimation techniques for advanced battery management systems — part i: Soc estimation," in *Proceedings of American Control Conference*, 2012, pp. 559–565.

[S46] S. J. Moura, N. A. Chaturvedi, and M. Krstić, "Adaptive partial differential equation observer for battery state-of-charge/state-of-health estimation via an electrochemical model," *ASME Journal of Dynamic Systems, Measurement, and Control*, vol. 136, no. 1, pp. 011 015–011 015–11, 2013.

[S47] R. Klein, N. Chaturvedi, J. Christensen, J. Ahmed, R. Findeisen, and A. Kojic, "Electrochemical model based observer design for a Lithium-ion battery," *IEEE Transactions on Control Systems Technology*, vol. 21, no. 2, pp. 289–301, 2013.

[S48] S. Tang, Y. Wang, Z. Sahinoglu, T. Wada, S. Hara, and M. Krstic, "State-of-charge estimation for lithium-ion batteries via a coupled thermal-electrochemical model," in *Proceedings of American Control Conference*, 2015, pp. 5871–5877.

[S49] N. Lotfi and R. Landers, "Robust nonlinear observer for state of charge estimation of Li-ion batteries," in *Proceedings of ASME Dynamic Systems and Controls Conference*, 2012, pp. 15–20.

Sidebar 2: Extended Kalman Filter

A dynamic system subjected to the effects of noise is referred to as a stochastic dynamic system [S50], which is present in almost every engineering field. With the inclusion of noise, a stochastic system can have a behavior significantly differing from its deterministic counterpart. A significant research effort has thus been stimulated, since the seminal work by Einstein in [S51], to investigate such systems, including their behavior characterization, control and estimation. Because of the practical infeasibility to measure each state of a stochastic system, unknown state estimation has been undergoing several decades of active research and development. In this research field, the Kalman filtering techniques has established a lead, and in particular, the extended Kalman filter (EKF) has emerged as the most popular estimation tool for nonlinear dynamic systems. A brief overview of this technique is offered below.

Consider

$$\begin{cases} x_{k+1} = f(x_k) + w_k, \\ \\ y_k = h(x_k) + v_k, \end{cases} \tag{S1}$$

where $x_k \in \mathbb{R}^{n_x}$ is the unknown system state, $y_k \in \mathbb{R}^{n_y}$ the output, and $\{w_k\}$ and $\{v_k\}$ noise sequences assumed to be Gaussian white with covariances of Q and R, respectively. The nonlinear mappings $f : \mathbb{R}^{n_x} \to \mathbb{R}^{n_x}$ and $h : \mathbb{R}^{n_x} \to \mathbb{R}^{n_y}$ represent, respectively, the process and measurement models. The EKF produces the estimate of x_k sequentially through time when the measurement y_k becomes available. It consists of two steps, prediction and update. The one-step-forward prediction yields the estimate of x_k, denoted as $\hat{x}_{k|k-1}$, using the measurements collected up to time $k-1$. Then upon the arrival of y_k, $\hat{x}_{k|k-1}$ will be updated to $\hat{x}_{k|k}$ leveraging the information conveyed by y_k about x_k. In the meantime, the estimation error covariances associated with both

estimates are computed accordingly.

When the state estimate $\hat{x}_{k-1|k-1}$ is generated, consider the first-order Taylor expansion of $f(x_{k-1})$ at this point:

$$f(x_{k-1}) \approx f(\hat{x}_{k-1|k-1}) + F_{k-1}\left(x_{k-1} - \hat{x}_{k-1|k-1}\right),\ F_{k-1} = \left.\frac{\partial f}{\partial x}\right|_{\hat{x}_{k-1|k-1}}. \tag{S2}$$

Then one can make the one-step-forward prediction through

$$\hat{x}_{k|k-1} = f\left(\hat{x}_{k-1|k-1}\right), \tag{S3}$$

$$P_{k|k-1} = F_{k-1}P_{k-1|k-1}F_{k-1}^{\top} + Q, \tag{S4}$$

where $P_{k|k-1}$ is the prediction error covariance quantifying the uncertainty of $\hat{x}_{k|k-1}$. After $\hat{x}_{k|k-1}$ is produced, it will be of next interest to investigate the updated state estimate. When the new measurement y_k becomes available, the update step can be performed as follows:

$$\hat{x}_{k|k} = \hat{x}_{k|k-1} + \underbrace{P_{k|k-1}H_k^{\top}\left(H_kP_{k|k-1}H_k^{\top} + R\right)^{-1}}_{\text{Kalman gain}}\left[y_k - h\left(\hat{x}_{k|k-1}\right)\right], \tag{S5}$$

$$P_{k|k} = P_{k|k-1} - P_{k|k-1}H_k^{\top}\left(H_kP_{k|k-1}H_k^{\top} + R\right)^{-1}H_kP_{k|k-1}, \tag{S6}$$

where H_k is obtained by linearization of $h(x_k)$, that is,

$$H_k = \left.\frac{\partial h}{\partial x}\right|_{\hat{x}_{k|k-1}}.$$

From above, the EKF consists of (S3)-(S4) for prediction and (S5)-(S6) for update. It addresses the nonlinearities through linearization of the system functions and then adapt the linear KF to the linearization. A schematic diagram of the EKF is shown in Fig. S1.

Since 1960s the EKF has gained wide use in the areas of aerospace, robotics, and biomedical, chemical, electrical and civil engineering, achieving great success in numerous

real-world applications. This is often ascribed to its conceptual straightforwardness as an extension of the linear KF and consequently, its relative easiness of design and execution. Another important reason is its good convergence from a theoretical viewpoint. In spite of the linearization-induced errors, the EKF has provable stability, see [S53]–[S56], under some conditions that can be satisfied by many practical systems. However, the EKF also suffers from some shortcomings. The foremost one is the inadequacy of its first-order accuracy for highly nonlinear systems. In addition, the need for explicit derivative matrices not only renders the EKF futile for discontinuous or other non-differentiable systems, but sometimes also pulls it away from convenient use in view of programming and debugging, especially when nonlinear functions of complex structure are faced. This factor, together with the computational complexity at $O(n_x^3)$, limits the application of EKF mostly to low-dimensional systems. It should be pointed out, however, that many practical systems are not complicated in terms of both dimensions and nonlinearities or can be simplified without much loss of model integrity. As a result, the EKF can be applied effectively to a large number of estimation problems and thus is widely regarded as the most popular estimation technique.

Some modified EKFs have also been developed for improved accuracy or efficiency in the past years. In this regard, a natural extension is through the second-order Taylor expansion, which will lead to the *second-order EKF* with more accurate estimation [S57]–[S59]. Another important variant, named *iterated EKF (IEKF)*, iteratively refines the state estimate around the current point at each time instant [S60], [S61]. Though coming at the expense of an increased computational cost, it can achieve higher estimation accuracy even in the presence of severe nonlinearities ingrained in systems.

References

[S50] A. Longtin, "Stochastic dynamical systems," vol. 5, no. 4, pp. 1619, 2010.

[S51] A. Einstein, "On the movement of small particles suspended in stationary liquids required by the molecular-kinetic theory of heat," *Annalen der Physik*, vol. 17, no. 4, pp. 549–560, 1905.

[S52] Wikipedia contributors. (2016, April 20/2016). Kalman filter. [Online]. Available: https://en.wikipedia.org/wiki/Kalman_filter.

[S53] M. Boutayeb, H. Rafaralahy, and M. Darouach, "Convergence analysis of the extended Kalman filter used as an observer for nonlinear deterministic discrete-time systems," *IEEE Transactions on Automatic Control*, vol. 42, no. 4, pp. 581–586, 1997.

[S54] A. Krener, "The convergence of the extended Kalman filter," in *Directions in Mathematical Systems Theory and Optimization*, A. Rantzer and C. Byrnes, Eds. Springer, 2003, vol. 286, pp. 173–182.

[S55] S. Kluge, K. Reif, and M. Brokate, "Stochastic stability of the extended Kalman filter with intermittent observations," *IEEE Transactions on Automatic Control*, vol. 55, no. 2, pp. 514–518, 2010.

[S56] S. Bonnabel and J.-J. Slotine, "A contraction theory-based analysis of the stability of the deterministic extended Kalman filter," *IEEE Transactions on Automatic Control*, vol. 60, no. 2, pp. 565–569, 2015.

[S57] H. Tanizaki, *Nonlinear Filters: Estimation and Applications*. Springer-Verlag Berlin Heidelberg, 1996.

[S58] S. Särkkä, *Bayesian Filtering and Smoothing*. Cambridge University Press, 2013.

[S59] M. Roth and F. Gustafsson, “An efficient implementation of the second order extended Kalman filter,” in *Proceedings of the 14th International Conference on Information Fusion*, 2011, pp. 1–6.

[S60] A. H. Jazwinski, *Stochastic processes and filtering theory*. New York, NY, USA: Academic Press, 1970.

[S61] B. Bell and F. Cathey, “The iterated Kalman filter update as a Gauss-Newton method,” *IEEE Transactions on Automatic Control*, vol. 38, no. 2, pp. 294–297, 1993.

Sidebar 3: Two-Stage Extended Kalman Filter

The two-stage EKF aims to reduce the computational cost of the joint EKF while maintaining comparable performance. The basic idea is that the computational complexity can be reduced by decomposing the high-order joint EKF into multiple low-order filters. This notion has been employed to develop a two-stage Kalman filter (KF) in [S62], where the KF is decomposed into two parallel but coupled reduced-order filters. Due to its ad-hoc decomposition, the two-stage KF is not exactly equivalent to the KF and therefore sub-optimality arises. An optimal two-stage KF (OTSKF) is developed and mathematically equivalent to the KF [S63]. The OTSKF applies linear state transformations to diagonalize the estimation error covariance matrices, and achieves a complete decoupling of two reduced-order filters. The state transformation-based diagonalization and decoupling stimulate extensions of the OTSKF, such as the OTSKF for time-varying and disturbance-driven systems [S64], [S65], the multi-stage KF [S66], the optimal two-stage EKF (OTSEKF) for nonlinear systems [S67], and the optimal two-stage EKF for linear parametric-varying systems [S68]. It is noteworthy that the OTSEKF involves nonlinear state transformations, and thus incurs a relatively high computation burden.

Consider a nonlinear discrete-time system

$$\begin{aligned} x_{k+1} &= f(x_k, \theta_k, u_k) + w_k^x, \\ y_k &= h(x_k, \theta_k, u_k) + v_k, \\ \theta_{k+1} &= g(\theta_k) + w_k^\theta, \end{aligned} \tag{S7}$$

where $x_k \in \mathbb{R}^{n_x}$ is the system state, $\theta_k \in \mathbb{R}^{n_\theta}$ the parameter, $y_k \in \mathbb{R}^{n_y}$ the output, $u_k \in \mathbb{R}^{n_u}$ the input, $f : \mathbb{R}^{n_x} \times \mathbb{R}^{n_\theta} \times \mathbb{R}^{n_u} \to \mathbb{R}^{n_x}$, $h : \mathbb{R}^{n_x} \times \mathbb{R}^{n_\theta} \times \mathbb{R}^{n_u} \to \mathbb{R}^{n_y}$ and $g : \mathbb{R}^{n_\theta} \to \mathbb{R}^{n_\theta}$. The sequences $\{w_k^x\}$, $\{w_k^\theta\}$ and $\{v_k\}$ are zero-mean Gaussian random processes with covariance matrices of Q_k^x,

Q_k^θ and R_k, respectively, and $\{w_k^x\}$, $\{w_k^\theta\}$ and $\{v_k\}$ are independent of each other. System (S7) is also referred as the augmented system with the augmented state $x_k^a = [x_k^\top, \theta_k^\top]^\top$. The joint EKF for the augmented system can be designed as described in Sidebar 2.

Assume that the two-stage EKF has state estimates $\hat{x}_{k|k}^a, \hat{x}_{k|k-1}^a$, covariance matrices $P_{k|k}^a, P_{k|k-1}^a$, and the gain matrix K_k^a. Next is to derive formula of the two-stage EKF. Different from the OTSEKF, the two-stage EKF adopts linear state transformations $\bar{x}_{k|k-1}^a = T(-U_k)\hat{x}_{k|k-1}^a$ and $\bar{x}_{k|k}^a = T(-V_k)\hat{x}_{k|k}^a$ to block-diagonalize covariance matrices $P_{k|k}^a$ and $P_{k|k-1}^a$, respectively. As in [S63], the transformation matrices take the form of

$$T(M) = \begin{bmatrix} I^{n_x \times n_x} & M \\ 0 & I^{n_\theta \times n_\theta} \end{bmatrix},$$

where $M \in \mathbb{R}^{n_x \times n_\theta}$ is the argument matrix to be determined. Note that $T^{-1}(M) = T(-M)$. In the transformed state coordinates, $P_{k|k-1}^a$, $P_{k|k}^a$, and K_k^a are given by

$$\bar{P}_{k|k-1}^a = T(-U_k) P_{k|k-1}^a T(-U_k)^\top,$$

$$\bar{P}_{k|k}^a = T(-V_k) P_{k|k}^a T(-V_k)^\top,$$

$$\bar{K}_k^a = T(-V_k) K_k^a.$$

Matrices $\bar{P}_{k|k-1}^a$ and $\bar{P}_{k|k}^a$ become block-diagonal, and thus two reduced-order filters are decoupled.

The two-stage EKF estimation for the augmented system can be performed in the new state coordinates. Fig. S2 shows the two-stage EKF scheme, which is summarized as follows.

Initialization: given the initial conditions (ICs) $\hat{x}_{0|0}^a = [\hat{x}^\top, \hat{\theta}^\top]^\top$ and $P_{0|0}^a$, the ICs for the two-stage EKF in the transformed coordinates can be obtained as: $\bar{P}_{0|0}^\theta = P_{0|0}^\theta, V_0 = P_{0|0}^{x\theta}(P_{0|0}^\theta)^{-1}, \bar{\theta}_{0|0} = \hat{\theta}_{0|0}, \bar{x}_{0|0} = \hat{x}_{0|0} - V_0\bar{\theta}_{0|0}, \bar{P}_{0|0}^x = P_{0|0}^x - V_0 P_{0|0}^\theta V_0^\top$. Matrices $P_{0|0}^x$ and $P_{0|0}^\theta$ are the

initial error covariance matrices of the state and parameter, respectively, and $P^{x\theta}_{0|0}$ is the initial error cross-covariance matrix between the state and parameter.

State and parameter prediction: by linearization of f and g at $(\hat{x}_{k|k}, \hat{\theta}_{k|k}, u_k)$, and h at $(\hat{x}_{k+1|k}, \hat{\theta}_{k+1|k}, u_k)$, compute matrices $A_k = \frac{\partial f}{\partial x_k}$, $B^{\theta}_k = \frac{\partial f}{\partial \theta_k}$, $B^{u}_k = \frac{\partial f}{\partial u_k}$, $G_k = \frac{\partial g}{\partial \theta_k}$, $C_k = \frac{\partial h}{\partial x_k}$, $D^{\theta}_k = \frac{\partial h}{\partial \theta_k}$, $D^{u}_k = \frac{\partial h}{\partial u_k}$, and

$$
\begin{aligned}
\bar{x}_{k|k-1} =& f(\bar{x}_{k-1|k-1}, \bar{\theta}_{k-1|k-1}, u_{k-1}) + (A_{k-1}V_{k-1} - U_k G_k)\bar{\theta}_{k-1|k-1},\\
\bar{\theta}_{k|k-1} =& g(\bar{\theta}_{k-1|k-1}),\\
\bar{P}^{x}_{k|k-1} =& A_{k-1}\bar{P}^{x}_{k-1|k-1}A^{\top}_{k-1} + \bar{Q}^{x}_{k},\\
\bar{Q}^{x}_{k} =& Q^{x}_{k-1} - \bar{U}_k (Q^{\theta}_{k-1})^{\top},\\
U_k =& \bar{U}_k - \bar{U}_k Q^{\theta}_k (P^{\theta}_{k|k-1})^{-1},\\
\bar{U}_k =& (A_{k-1}V_{k-1} + B^{\theta}_{k-1})G^{-1}_{k-1},\\
\bar{P}^{\theta}_{k|k-1} =& G_{k-1}\bar{P}^{\theta}_{k-1|k-1}G^{\top}_{k-1} + Q^{\theta}_{k-1}.
\end{aligned}
$$

State and parameter update:

$$
\begin{aligned}
\bar{K}^{x}_k =& \bar{P}^{x}_{k|k-1}C^{\top}_k (C_k \bar{P}^{x}_{k|k-1}C^{\top}_k + R_k)^{-1},\\
\bar{x}_{k|k} =& \bar{x}_{k|k-1} + \bar{K}^{x}_k (y_k - h(\bar{x}_{k|k-1}, \bar{\theta}_{k|k-1}, u_k),\\
\bar{P}^{x}_{k|k} =& \bar{P}^{x}_{k|k-1} - \bar{K}^{x}_k C_k \bar{P}^{x}_{k|k-1},\\
\bar{\theta}_{k|k} =& \bar{\theta}_{k|k-1} + \bar{K}^{\theta}_k (y_k - h(\bar{x}_{k|k-1}, \bar{\theta}_k, u_k)) - S_k \bar{\theta}_{k|k-1},\\
\bar{K}^{\theta}_k =& \bar{P}^{\theta}_{k|k-1}S^{T}_k (C_k \bar{P}^{x}_{k|k-1}C^{\top}_k + R_k + S^{T}_k \bar{P}^{\theta}_{k|k-1}S^{T}_k)^{-1},\\
\bar{P}^{\theta}_{k|k} =& \bar{P}^{\theta}_{k|k-1} - \bar{K}^{\theta}_k S_k \bar{P}^{\theta}_{k|k-1},
\end{aligned}
$$

$$S_k = C_k U_k + D_k^{\theta},$$

$$V_k = U_k - \bar{K}_k^x S_k.$$

The state estimate $\hat{x}^a$ can be recovered by the inverse two-stage state transformation as: $\hat{x}^a_{k|k-1} = T(U_k)\bar{x}^a_{k|k-1}, \hat{x}^a_{k|k} = T(V_k)\bar{x}^a_{k|k}$.

References

[S62] B. Friedland, "Treatment of bias in recursive filtering," *IEEE Trans. Automat. Control*, vol. 14, no. 4, pp. 359-367, Aug 1969.

[S63] C.-S. Hsieh and F.-C. Chen, "Optimal solution of the two-stage kalman estimator," *IEEE Trans. Automat. Control*, vol. 44, no. 1, pp. 194–199, 1999.

[S64] ——, "General two-stage kalman filters," *IEEE Trans. Automat. Control*, vol. 45, no. 4, pp. 819–824, 2000.

[S65] C.-S. Hsieh, "Robust two-stage kalman filters for systems with unknown inputs," *IEEE Trans. Automat. Control*, vol. 45, no. 12, pp. 2374–2378, 2000.

[S66] F.-C. Chen and C.-S. Hsieh, "Optimal multistage kalman estimators," *IEEE Trans. Automat. Control*, vol. 45, no. 11, pp. 2182–2188, 2000.

[S67] C.-S. Hsieh, "General two-stage extended kalman filters," *IEEE Trans. Automat. Control*, vol. 48, no. 2, pp. 289–293, 2003.

[S68] M. Hilairet, F. Auger, and E. Berthelot, "Speed and rotor flux estimation of induction machines using a two-stage extended kalman filter," *Automatica*, vol. 45, no. 8, pp. 1819–1827, 2009.

Sidebar 4: Observability for Nonlinear Systems

Observability, a fundamental system property, determines whether the system state can be reconstructed from measurements. Its precise characterization relies on the state indistinguishablility, which is defined as follows

Definition 0.1 (State Indistinguishablility): [S69] Consider a nonlinear control system

$$\begin{aligned} \dot{\zeta} &= f(\zeta, u), \\ y &= h(\zeta), \end{aligned} \tag{S8}$$

where $\zeta \in R^n$ is the system state, $u \in \mathbb{R}^m$ the control input, $y \in \mathbb{R}^p$ the output, and f, h are smooth. Two states ζ and $\bar{\zeta}$ are indistinguishable if for every input $u \in [0, T]$, the system outputs corresponding to two pairs (ζ, u) and $(\bar{\zeta}, u)$ are exactly the same.

A system carries the observability, or is observable, if it does not have indistinguishable states. Regarding a single output uncontrolled system, the observability verification is reduced to performing a simple algebraic test, which induces the following observability definition.

Definition 0.2 (Observability): [S70] The system

$$\begin{aligned} \dot{\zeta} &= f(\zeta), \ \zeta \in \mathbb{R}^n, \\ y &= h(\zeta), \ y \in \mathbb{R}, \end{aligned} \tag{S9}$$

is said to be locally observable in U_0, a neighborhood of the origin, if

$$\operatorname{rank}\{\mathrm{d}h(\zeta), \ldots, \mathrm{d}(L_f^{n-1} h(\zeta))\} = n, \quad \zeta \in U_0, \tag{S10}$$

where the function $L_f h(\zeta) = \frac{\partial h(\zeta)}{\partial \zeta} f(\zeta)$ is the *Lie derivative* of $h(\zeta)$ along $f(\zeta)$, and repeated Lie derivatives $L_f^k h(\zeta) = L_f(L_f^{k-1} h(\zeta))$, $k \geq 1$ with $L_f^0 h(\zeta) = h(\zeta)$. If (S10) holds for every $\zeta \in \mathbb{R}^n$, we say that the system is observable.

For a nonlinear control system (S8), the observability does not imply that every input distinguishes arbitrary system states, and thus is input-dependent. The input-dependent observability is mathematically rigorous, but provides little guidance in observer synthesis. Practically, people are interested in finding out: whether the system is observable for a given control input [S71], or whether the observability is input-independent [S70]. Given a control input, the verification of observability for system (S8) is straightforward by following Definition 0.2. The input-independent observability, named after uniform observability, is important and interesting because it enables a fruitful of observer designs for bilinear systems [S72], affine control systems [S70], non-affine control systems [S71], etc. For a single input and single output (SISO) nonlinear system subject to an affine control input, it adopts the following uniform observability.

Definition 0.3 (Uniform Observability): [S70, Def. 2] The SISO controlled nonlinear system

$$\begin{aligned} \dot{\zeta} &= f(\zeta) + g(\zeta)u,\ x \in \mathbb{R}^n, \\ y &= h(\zeta), \end{aligned} \tag{S11}$$

is uniformly observable, if the system (S9) is observable, and the system (S11) is observable for any input, i.e., on any finite time interval $[0,T]$, for any measurable bounded input $u(t)$ defined on $[0,T]$, the initial state is uniquely determined on the basis of the output $y(t)$ and the input $u(t)$.

Verifying uniform observability of a generic system is not easy except for certain special cases. For instance work [S70], [S73] establishes necessary and sufficient condition to guarantee a system (S8) with affine control inputs is uniformly observability.

References

[S69] R. Hermann and A. J. Krener, "Nonlinear controllability and observability," *IEEE Trans. Automat. Control*, vol. AC-22, no. 5, pp. 728–740, Oct. 1977.

[S70] J. P. Gauthier and H. Hammouri and S. Othman, "A simple observer for nonlinear systems–applications to bioreactors," *IEEE Trans. Automat. Control*, vol. 37, no. 6, pp. 875–880, 1992.

[S71] E. Busvelle and J. P. Gauthier, "High-gain and non-high-gain observers for nonlinear systems," *Contemporary Trends in Nonlinear Geometric Control Theory*, pp. 257–286, 2002.

[S72] D. Williamson, "Observation of bilinear systems with application to biological control," *Automatica*, vol. 13, pp. 243–254, 1977.

[S73] J. P. Gauthier and I. Kupka, *Deterministic Observation Theory and Applications*. UK: Cambridge University Press, 2001.

Author Information

Yebin Wang (yebinwang@ieee.org) is a Senior Principal Research Scientist at Mitsubishi Electric Research Laboratories in Cambridge, MA, USA. He received the B.Eng. degree in Mechatronics Engineering from Zhejiang University, Hangzhou, China, in 1997, M.Eng. degree in Control Theory & Control Engineering from Tsinghua University, Beijing, China, in 2001, and Ph.D. in Electrical Engineering from the University of Alberta, Edmonton, Canada, in 2008. His research interests include nonlinear control and estimation, optimal control, adaptive systems and their applications including mechatronic systems. He was a Software Engineer, Project Manager, and Manager of R&D Dept. in industries, Beijing, China. He can be contacted at Mitsubishi Electric Research Laboratories, 201 Broadway, Cambridge, MA 20139, USA.

Huazhen Fang is an Assistant Professor in the Department of Mechanical Engineering at the University of Kansas. His broad research interest lies in dynamic systems and control, with a recent application focus on energy management. He received Ph.D. in Mechanical Engineering in 2014 from the Department of Mechanical & Aerospace Engineering, University of California, San Diego, with specialization in Dynamic Systems and Control. Prior, he received M.Sc. in Mechanical Engineering from the University of Saskatchewan, Saskatoon, Canada in 2009, and B.Eng. in Computer Science & Technology from Northwestern Polytechnic University, Xi'an, China, in 2006.

Lei Zhou received the B.S. degree from the Department of Precision Instrument and Mechanology, Tsinghua University, China, in 2012, and received S.M. degree from the Department of Mechanical Engineering at Massachusetts Institute of Technology (MIT) in 2014. She is currently

working toward the Ph.D. degree at the Department of Mechanical Engineering at MIT. Her research interests include control, estimation and precision mechatronics.

Toshihiro Wada received the B.Eng. degree in informatics and mathematical science and the M. Informatics degree in Applied Analysis and Complex Dynamical Systems from the Kyoto University, Kyoto, Japan, in 2005 and 2007 respectively. His current research interests include sensing and optimization of battery systems.